A Unified Jet Model of X-Ray Flashes, X-Ray-Rich GRBs, and GRBs

D. Q. Lamb

d-lamb@uchicago.edu

T. Q. Donaghy

quinn@uchicago.edu

C. Graziani

carlo@kazoo.uchicago.edu

Department of Astronomy and Astrophysics, University of Chicago

ABSTRACT

HETE-2 has provided strong evidence that the properties of X-Ray Flashes (XRFs) and GRBs form a continuum, and therefore that these two types of bursts are the same phenomenon. We show that both the universal jet and the uniform jet models can explain the observed properties of GRBs reasonably well. However, if one tries to account for the properties of both XRFs and GRBs in a unified picture, the uniform jet model works reasonably well while the universal jet model fails utterly. The uniform jet model of XRFs and GRBs implies that most GRBs have very small jet opening angles ($\sim$ half a degree). This suggests that magnetic fields play a crucial role in GRB jets. The model also implies that the energy radiated in gamma rays is ~ 100 times smaller than has been thought. Most importantly, the model implies that there are $\sim 10^4 - 10^5$ more bursts with very small jet opening angles for every such burst we see. Thus the rate of GRBs could be comparable to the rate of Type Ic core collapse supernovae. Accurate, rapid localizations of many XRFs, leading to identification of their X-ray and optical afterglows and the determination of their redshifts, will be required in order to confirm (or refute) these profound implications. HETE-2 is ideally suited to do this (it has localized 16 XRFs in $\sim$ 2 years), whereas *Swift* is not. The unique insights into the structure of GRB jets, the rate of GRBs, and the nature of Type Ic supernovae that XRFs may provide therefore constitute a compelling scientific case for continuing HETE-2 during the *Swift* mission.

Subject headings: gamma rays: bursts – supernovae

1. Introduction

Two-thirds of all HETE-2–localized bursts are either "X-ray-rich" or X-Ray Flashes (XRFs); of these, one-third are XRFs [1] (Sakamoto et al. 2003b). The latter have received increasing attention in the past several years (Heise et al. 2000; Kippen et al. 2002), but their nature remains unknown.

XRFs have t_{90} durations between 10 and 200 sec and their sky distribution is consistent with isotropy. In these respects, XRFs are similar to "classical" GRBs. A joint analysis of WFC/BATSE spectral data showed that the low-energy and high-energy photon indices of XRFs are -1 and ~ -2.5, respectively, which are similar to those of GRBs, but that the XRFs had spectral peak energies $E^{\rm obs}_{\rm peak}$ that were much lower than those of GRBs (Kippen et al. 2002). The only difference between XRFs and GRBs therefore appears to be that XRFs have lower $E^{\rm obs}_{\rm peak}$ values. It has therefore been suggested that XRFs might represent an extension of the GRB population to bursts with low peak energies.

In this paper, we explore a unified picture of XRFs and GRBs, motivated by HETE-2 (Ricker et al. 2003a) observations of these high-energy events. In the uniform jet model, the different properties of these kinds of bursts are due to the differences in the solid angle $ojet$ of the jet. We show that this simple model can account for a wealth of observations of these high-energy events. In contrast, we find that, although the universal or structured jet model can can account reasonably well for the properties of GRBs, it cannot easily be extended to account for the observed properties of XRFs and X-ray-rich GRBs.

The uniform jet model of XRFs, X-ray-rich GRBs, and GRBs, implies that most GRBs have very small jet opening angles ($\sim$ half a degree). This suggests that magnetic fields play a crucial role in GRB jets. The model also implies that the energy radiated in gamma rays is $\sim$ 100 times smaller than has been thought. Most importantly, the model implies that there are $\sim 10^4 - 10^5$ more bursts with very small jet opening angles for every such burst we see. Thus the rate of GRBs could be comparable to the rate of Type Ic core collapse supernovae.

This paper is organized as follows. In §2, we summarize the results of HETE-2 observations of XRFs and GRBs. In §3, we define the uniform jet and the universal or structured jet models. In §4, we describe our simulations; in particular, we describe how we model the bursts themselves, propagate them to the Earth, and model the instruments that detect them. In §5, we describe our results and compare them with observations. In §7, we discuss

---

[1] We define "X-ray-rich" GRBs and XRFs as those events for which $\log[S_X(2-30\ {\rm kev})/S_\gamma(30-400\ {\rm kev})] > -0.5$ and 0.0, respectively.

their implications. Section 8 summarizes our conclusions.

2. Observations of XRFs and GRBs

2.1. HETE-2 Results

Clarifying the nature of XRFs and their connection to GRBs could provide a breakthrough in our understanding of the prompt emission of GRBs. Analyzing 42 X-ray-rich GRBs and XRFs seen by the FREGATE (Atteia et al. 2003) and/or the WXM (Kawai et al. 2003) instruments on HETE-2, Sakamoto et al. (2003b) find that XRFs, X-ray-rich GRBs, and GRBs form a continuum in the $[S_\gamma(2-400 \text{ kev}), E_{\rm peak}^{\rm obs}]$-plane (see Figure 1), where $S_\gamma(2-400 \text{ kev})$ is the fluence of the burst in the 2-400 keV energy band and $E_{\rm peak}^{\rm obs}$ is the energy of the peak of the burst spectrum in νF_ν. This result, when combined with the earlier results described above, strongly suggests that all of these events are the same phenomenon.

Furthermore, Lamb et al. (2003) have placed 9 HETE-2 GRBs with known redshifts and 2 XRFs with known redshifts or strong redshift constraints in the $(E_{\rm iso}, E_{\rm peak})$-plane (see Figure 2). Here $E_{\rm iso}$ is the isotropic-equivalent burst energy and $E_{\rm peak}$ is the energy of the peak in the burst νF_ν spectrum, measured in the source frame. The HETE-2 bursts confirm the relation between $E_{\rm iso}$ and $E_{\rm peak}$ found for GRBs by Lloyd-Ronning, Petrosian, & Mallozzi (2000) using BATSE GRBs and by Amati et al. (2002) using *Beppo*SAX GRBs, and extend it down in $E_{\rm iso}$ by a factor of ~ 300. The fact that XRF 020903 (Sakamoto et al. 2003a), one of the softest events localized by HETE-2 to date, and XRF 030723 (Ricker et al. 2003b), the most recent XRF localized by HETE-2, lie squarely on this relation (Lamb et al. 2003), provides additional strong evidence that XRFs and GRBs are the same phenomenon. However, additional redshift determinations are clearly needed for XRFs with 1 keV $< E_{\rm peak} <$ 30 keV in order to confirm these results.

Lamb et al. (2003) have shown, using HETE-2 and *Beppo*SAX GRBs with known redshifts or strong redshift constraints, that there is also a relation between the isotropic-equivalent burst luminosity L_γ and $E_{\rm peak}$ extending over five decades in L_γ, and (as must then be the case) between $E_{\rm iso}$ and L_γ extending over five decades (see Figure 2).

The origin of the correlations between $E_{\rm iso}$ and $E_{\rm peak}$ found by Lloyd-Ronning, Petrosian, & Mallozzi (2000) and Amati et al. (2002), and the correlations between L_γ and $E_{\rm peak}$, and $E_{\rm iso}$ and L_γ found by Lamb et al. (2003) – especially the tightness of the correlations – is not understood at the present time. In the simple external shock model of GRBs, no strong correlations are expected (Dermer, Chiang, & Böttcher 1999a). However, more complex scenarios within the external shock model can produces a correlation (Dermer 1999b). In the internal shock model, one expects $E_{\rm iso} \propto E_{\rm peak}^{1/2}$, but with a substantial dispersion due to differences in the bulk Lorenz factor γ of the plasma in the jet and the relative Lorenz factors $\gamma_{\rm int}$ of the colliding shells Lloyd-Ronning, Petrosian, & Mallozzi (2000).

2.2. Evidence That Most GRBs Have a "Standard" Energy

Frail et al. (2001; see also Bloom et al. 2003) find that most GRBs have a "standard" energy; i.e, if their isotropic equivalent energy is corrected for the jet opening angle $\theta_{\rm jet}$ inferred from the jet break time, most GRBs have the same radiated energy, $E_\gamma = 1.3 \times 10^{51}$ ergs, to within a factor $\pm$ 2-3. This is illustrated in Figure 3, which shows distribution of isotropic-equivalent energies $E_{\rm iso}$ (top panel) and the resulting distribution of total radiated energy in gamma-rays E_γ, taking into account the jet opening angle inferred from the jet break time (bottom panel).

Pursuing this picture further, we plot in Figure 4 the distribution of $E_{\rm iso}$, L_γ, and $E_{\rm peak}$ as a function of $\Omega_{\rm jet}$ for the HETE-2 and *Beppo*SAX GRBs with known redshifts or strong redshift constraints. Figure 4 shows that all three quantities are strongly correlated with $ojet$. The correlation of $E_{\rm iso}$ with $ojet$ is implied by Frail et al.'s and Bloom, Frail, & Kulkarni's finding that most GRBs have a "standard" energy. The correlation of $E_{\rm peak}$ with $ojet$ is implied by this finding and the relation between $E_{\rm iso}$ and $E_{\rm peak}$ found by Lloyd-Ronning, Petrosian, & Mallozzi (2000) and Amati et al. (2002).

The strength of the correlations of all three quantities with $ojet$ lends strong additional support to a picture in which most GRB have a standard energy and the range of $\sim 10^5$ in $E_{\rm iso}$ and L_γ that is observed is due either to differences in the viewing angle $\theta_{\rm view}$ of the observer with respect to the axis of the jet or to differences in the jet opening angle $\theta_{\rm jet}$'. We pursue these possibilities below.

3. Jet Models of GRBs

Two models of GRB jets have received widespread attention:

- The universal or structured jet model (see the left-hand panel of Figure 5). In this model, all GRBs produce jets with the same structure (Rossi, E., Lazzati, D, & Rees, M. J. 2002; Woosley, Zhang, & Heger 2003; Zhang & Mészáros 2002; Mészáros, Ramirez-Ruiz, Rees, & Zhang 2002). The isotropic-equivalent energy $E_{\rm iso}$ and luminosity L_γ is assumed to decrease as the viewing angle $\theta_{\rm view}$, as measured from the jet axis, increases.

The wide range in values of $E_{\rm iso}$ is then attributed to differences in the viewing angle $\theta_{\rm view}$. In order to recover the "standard energy" result (Frail et al. 2001; Bloom, Frail & Kulkarni 2003), $E_{\rm iso}(\theta_{\rm view}) \propto \theta_{\rm view}^{-2}$ is required (Rossi, E., Lazzati, D, & Rees, M. J. 2002; Zhang & Mészáros 2002).

- The uniform jet model (see the right-hand panel of Figure 5). In this model, GRB jets have a wide range of jet opening angles $\theta_{\rm jet}$ (Frail et al. 2001). For $\theta_{\rm view} < \theta_{\rm jet}$, $E_{\rm iso}(\theta_{\rm view}) \approx$ constant, while for $\theta_{\rm view} > \theta_{\rm jet}$, $E_{\rm iso}(\theta_{\rm view}) = 0$. The wide range in values of $E_{\rm iso}$ is then attributed to differences in the jet opening angle $\theta_{\rm jet}$. This is the model that Frail et al. (2001) and Bloom, Frail & Kulkarni (2003) assume in deriving a "standard energy" for most bursts.

Motivated by the HETE-2 results showing that the relation between $E_{\rm iso}$ and $E_{\rm peak}$ extends over at least five decades and appears to hold for XRFs and X-ray-rich GRBs, as well as for GRBs; the finding by Frail et al. (2001) that most GRBs have a standard energy; and the strong correlations we find between $\Omega_{\rm jet}$ and $E_{\rm iso}$, L_γ, and $E_{\rm peak}$, we make three key assumptions in exploring a unified jet picture of all three kinds of bursts:

1. We assume that most GRBs have a standard energy. In the uniform jet model, this means that if the isotropic-equivalent energy $E_{\rm iso}$ of the GRB is corrected for the jet opening angle $\theta_{\rm jet}$ inferred from the jet break time, most GRBs will have the same energy, to within a factor of $\pm 2-3$ (Frail et al. 2001; Bloom, Frail & Kulkarni 2003). In the universal jet model, this requires $E_{\rm iso}(\theta_{\rm view}) \propto \theta_{\rm view}^{-2}$, as we have already mentioned.

2. We assume that most GRB spectra obey the relation (Lloyd-Ronning, Petrosian, & Mallozzi 2000; Amati et al. 2002; Lamb et al. 2003):

$$E_{\rm peak} \propto (E_{\rm iso})^{1/2} \; , \qquad (1)$$

   and that this relation holds for XRFs and X-ray-rich GRBs, as well as for GRBs.

3. We assume that the range of $\sim 10^5$ in $E_{\rm iso}$ and L_γ that is observed is due either to differences in the viewing angle $\theta_{\rm view}$ of the observer with respect to the axis of the jet (as the universal jet model posits) or to differences in the jet opening angle $\theta_{\rm jet}$ (as the uniform jet model posits).

4. Simulations of Gamma-Ray Bursts

We begin by giving an overview of our simulations of observed GRBs before describing them in detail mathematically. Our overall approach is to simulate the GRBs that are observed by different instruments by (1) modeling the bursts in the source frame; (2) propagating the bursts from the source frame to us, using the cosmology that we have adopted; and (3) determining the bursts that are observed, using the properties of the instruments that observe them.

This logical sequence is evident in Figure 6, which shows a flowchart of the calculations involved in our simulations of bursts in the uniform jet model. For each simulated burst we obtain a redshift z and a jet opening solid angle ($\Omega_{\rm jet}$) by drawing from specific distributions (blue boxes). In addition, we introduce three log-normal smearing functions (maroon boxes) to generate a timescale (T), a jet energy (E_γ) and a coefficient for the Amati relation (C). Using these five quantities, we calculate various rest-frame quantities ($E_{\rm iso}$, $E_{\rm peak}$, etc.). Finally, we construct a Band spectrum for each burst and transform it into the observer frame, which allows us to calculate fluences and peak fluxes and to determine if the burst would be detected by various experiments.

Given this procedure, it is a simple matter to simulate the observed distributions of GRBs for the universal jet model, simply by making the substitution $\Omega_{\rm jet} \to \Omega_{\rm view}$. However, in the case of the universal jet model, δ is not free, but must be 2, in order to recover the results of Frail et al. (2001) and Bloom, Frail & Kulkarni (2003) [see, e.g., Rossi, E., Lazzati, D, & Rees, M. J. (2002); Zhang & Mészáros (2002)].

4.1. GRB Rest-Frame Quantities

4.1.1. Uniform Jet Model

The distribution in jet opening solid angle $\Omega_{\rm jet}$ generates our GRB luminosity function; we are primarily interested in a power-law distribution, although we briefly consider Gaussian and exponential distributions as well. We define the fraction of the sky subtended by the GRB jet to be

$$f_{jet} = \frac{\Omega_{\rm jet}}{2\pi} = 1 - \cos\theta_{jet} \tag{2}$$

We define the true distribution of opening angles to be

$$f_{true}(\Omega_{\rm jet}) \propto (\Omega_{\rm jet})^{-\delta}. \tag{3}$$

We define the observed distribution of opening angles to be

$$f_{obs}(\Omega_{\rm jet}) \propto (\Omega_{\rm jet})^{-\delta_{\rm sim}} \propto f_{jet}^{-\delta_{\rm sim}}. \tag{4}$$

Since we observe only those bursts whose jets are oriented toward the earth, the observed distribution of opening angles is related to the true distribution of opening angles by

$$f_{obs} = \cdot f_{jet} f_{true}(\Omega_{\rm jet}) \propto (\Omega_{\rm jet})^{(1-\delta)} \tag{5}$$

We thus simulate bursts using the power-law index $\delta_{\rm sim}$ from which the true power-law index can be found using the relation $\delta = 1 + \delta_{\rm sim}$.

The isotropic-equivalent emitted energy $E_{\rm iso}$ is then given by

$$E_{\rm iso} = \frac{E_\gamma}{f_b} = \frac{E_\gamma}{\Omega_{\rm jet}/2\pi}, \tag{6}$$

where E_γ is the total radiated energy of the burst. We have reproduced the parameters of the Gaussian function derived by Bloom, Frail & Kulkarni (2003), using their sample of GRBs with observed jet break times (see Figure 8). We therefore draw values for E_γ randomly from the narrow Gaussian found by Bloom, Frail & Kulkarni (2003) and defined by

$$G(E_\gamma) = \exp\left(\frac{-(\log E_\gamma - \log E_\gamma^0)^2}{2\sigma_E^2}\right). \tag{7}$$

where $\log E_\gamma^0({\rm erg}) = 51.124$ and $\log \sigma_E = 0.35$ (see also Table 1)

We also include a mechanism for rescaling this central value (which is equivalent to a change in the range of $\Omega_{\rm jet}$, since only $E_{\rm iso}$ is observed).

Our simulations thus use the value of $E_\gamma^0 = 1.33 \times 10^{51}$ ergs found by Bloom, Frail & Kulkarni (2003). However, their sample contained no X-Ray Flashes, since no afterglows and therefore redshifts had been reported for XRFs prior to the HETE-2–localization of XRF 020903 Sakamoto et al. (2003a). The values of $E_{\rm iso}$ for XRFs 020903 and 030723 Lamb et al. (2003) are $\sim$ 100 times lower than the value of E_γ derived by Frail et al. (2001) and citebloom2003. Thus there is no value of the opening solid angle $\Omega_{\rm jet}$ that can accommodate these values of $E_{\rm iso}$. Since we are pursuing a unified jet model of XRFs, X-ray-rich GRBs, and GRBs, we must be able to accommodate values of $E_{\rm iso}$ that are $\sim$ 100 times smaller than the value of E_γ derived by Frail et al. (2001) and citebloom2003.

We therefore introduce an ability to rescale the central value of E_γ. In doing so, we note that the derivation of E_γ is dependent on the coefficient in front of the relation between the jet-break time and $\theta_{\rm jet}$, and that the value of this coefficient is uncertain (Rhoads 1999; Sari & Piran & Halpern 1999).

This rescaling of E_γ introduces an additional parameter into our model, $C_{\rm jet}$:

$$E_{\rm iso} = \frac{E_\gamma}{C_{\rm jet} \cdot \Omega_{\rm jet}/2\pi}. \tag{8}$$

XRF 020903 has a value $E_{\rm iso} = 2.3 \times 10^{49}$ ergs Sakamoto et al. (2003a), which requires that $C_{\rm jet}$ be at least 57.8; this choice is conservative in the sense that it implies that XRF 020903 lies at the faintest end of the range of possible values of $E_{\rm iso}$ values and has the maximum possible opening angle of $\Omega_{\rm jet} = 2\pi$. The brightest GRB in our sample is GRB 990123., which has a value $E_{\rm iso} = 2.8 \times 10^{54}$ ergs. Thus the range of $E_{\rm iso}$ is at least $\sim 10^5$, and so the range of $\Omega_{\rm jet}$) must also be $\sim 10^5$. Since only $E_{\rm iso}$ is a directly observable quantity, the exact value of $C_{\rm jet}$ is degenerate with the minimum value of $\Omega_{\rm jet}$. Thus GRB 990123 provides a constraint only on $C_{\rm jet} \cdot \Omega_{\rm jet}^{\rm min}$.

Since we wish our burst simulations to explain the full range of observed $E_{\rm iso}$, we require a range of approximately five decades in $\Omega_{\rm jet}$ (conservatively, from 2π to $2\pi \times 10^{-5}$ sr). We have then varied $C_{\rm jet}$ to best match the observed cumulative distributions shown in Figure 13, as determined by visual comparison of the observed and predicted cumulative distributions. The fiducial model that we use in this paper has a value of $C_{\rm jet} = 95.5$. This gives minimum and maximum values of $E_{\rm iso}$ of 1.4×10^{49} ergs and 1.4×10^{54} ergs. The latter value is slightly smaller than the value of $E_{\rm iso}$ for GRB 990123, but the range of simulated E_γ values, although narrow, is sufficient to account for this event and events like it. We have used the value $C_{\rm jet} = 95.5$ to rescale the $\Omega_{\rm jet}$ values reported by Bloom, Frail & Kulkarni (2003) (see Figure 11), which corresponds to rescaling the coefficient in the relation between the jet break time and $\theta_{\rm jet}$ to smaller values by a factor of ~ 10, and therefore also rescaling $\theta_{\rm jet}$ to smaller angles by a factor of ~ 10.

In order to incorporate the relation between $E_{\rm iso}$ and $E_{\rm peak}$ found by Lloyd-Ronning, Petrosian, & Mallozzi (2000) and Amati et al. (2002), we use a second Gaussian smoothing function defined by

$$E_{\rm peak} = C \cdot \left(\frac{E_{\rm iso}}{10^{52}{\rm erg}}\right)^s , \tag{9}$$

and a second Gaussian smoothing function, defined by

$$G(C) = \exp\left(\frac{-(\log C - \log C_0)^2}{2\sigma_C^2}\right). \tag{10}$$

We constrain s to equal 0.5. Then, fitting these equations to the HETE-2 and *Beppo*SAX GRBs with known redshifts (see Figures 2 and 8), we find best-fit parameters $C_0 = 90.4$ keV and $\sigma_C = 0.70$ (see also Table 1). We then draw randomly from this Gaussian distribution to choose the $E_{\rm peak}$ corresponding to the $E_{\rm iso}$ for a particular burst.

Finally, we require the timescale that converts burst fluence to peak flux. We determine this timescale by fitting a third Gaussian smoothing function, defined by

$$G(T) = \exp\left(\frac{-(\log T - \log T_0)^2}{2\sigma_T^2}\right) , \tag{11}$$

to the distribution of the ratio $E_{\rm iso}/L_\gamma$ for the HETE-2 and *Beppo*SAX bursts with known redshifts (see Figure 8). We find best-fit parameters $T_0 = 3.41$ sec and $\sigma_T = 0.33$ (see also Table 1). We then draw randomly from this Gaussian distribution to convert the burst fluences to peak fluxes. We also employ this timescale to estimate the luminosities of the bursts, using the formula $L_\gamma = E_{\rm iso}/T$.

4.1.2. Universal Jet Model

In order to recover the "standard energy" result (Frail et al. 2001; Bloom, Frail & Kulkarni 2003), the universal jet model requires $E_{\rm iso} \propto \theta_{\rm view}^{-2}$ (Rossi, E., Lazzati, D, & Rees, M. J. 2002; Zhang & Mészáros 2002). This requirement allows us to simulate the universal jet model by simply making the substitution $\Omega_{\rm jet} \rightarrow \Omega_{\rm view}$ in our usual uniform jet simulations. To see this, compare Equation ??? with

$$E_{\rm iso} \propto \frac{1}{\theta_{\rm view}^2} \propto \frac{1}{\Omega_{\rm view}}, \tag{12}$$

Although the physical interpretations of the two equations are entirely different, they give the same results. In addition to this substitution, we have to specify the correct δ_{sim} for the universal jet model. Since the bursts are randomly oriented with respect to our line of sight, we draw $\Omega_{\rm view}$ values from a flat distribution, $d\Omega_{\rm view}$, which corresponds to $\delta_{sim} = 0$. Drawing from this distribution results in very few small $\Omega_{\rm view}$ values as compared with the large number of $\Omega_{\rm view}$ values near 2π. In this model, most bursts have $\theta_{\rm view} \sim 90°$, and consequently, the range of of $\Omega_{\rm view}$ values in logarithmic space is small. As a result, the universal jet model predicts that most of the bursts arriving at the Earth will have small values of $E_{\rm iso}$, L_γ, etc. (Rossi, E., Lazzati, D, & Rees, M. J. 2002).

We introduce the same ability to rescale the central value of E_γ in the universal jet model. For this model we consider two cases: in the first case, we "pin" the minimum value of $E_{\rm iso}$ (i.e., the value of $E_{\rm iso}$ corresponding to $\Omega_{\rm view} = 2\pi$) at the value for XRF 020903; in the other case, we "pin" the minimum value of $E_{\rm iso}$ to to the value for GRB 980326 (the smallest $E_{\rm iso}$ in out sample of HETE-2 and *Beppo*SAX bursts with known redshifts, apart from the XRFs). In the first case, we derive $C_{\rm jet} = 57.83$, and in the second $C_{\rm jet} = 0.237$. In the first case, the universal jet model is able to account for the full observed range of $E_{\rm iso}$, while in the second case, it can only account for the GRBs.

4.2. Gamma-Ray Burst Rate as a Function of Redshift

The rate of GRBs per redshift interval dz is given by

$$\rho(z) = R_{GRB}(z) \times (1+z)^{-1} \times 4\pi r(z)^2 \frac{dr}{dz} = \left[\frac{\mathrm{num}}{\mathrm{z \cdot year}}\right] , \tag{13}$$

where $R_{GRB}(z)$ is the rate of GRBs per comoving volume and $r(z)$ is the comoving distance to the source (see §4.3 below for the precise definition of $r(z)$). We use the phenomenological parameterization of the star formation rate as a function of redshift suggested by Rowan-Robinson (2001) to parameterize GRB rate as a function of redshift. In this parameterization, R_{GRB} is given by,

$$R_{GRB}(z) = R_0 \left(\frac{t(z)}{t(0)}\right)^P \exp\left[Q\left(1 - \frac{t(z)}{t(0)}\right)\right] = \left[\frac{\mathrm{num}}{\mathrm{year \cdot Gpc^3}}\right] . \tag{14}$$

Here, $t(z)$ is the elapsed time since the big bang at that redshift. In this paper, we adopt the values $P = 1.2$ and $Q = 2.5$, which provide a good fit to the existing data on the star-formation rate as a function of redshift. We then draw random redshifts from resulting star-formation rate (SFR) curves.

4.3. Cosmology

The Rowan-Robinson SFR model depends on a few basic cosmological parameters, as do the observed peak photon number and energy fluxes and fluences of the bursts. In this paper, we adopt the values $\Omega_M = 0.3$, $\Omega_\Lambda = 0.7$ and $H_0 = 65$ km s^{-1} Mpc^{-1}.

The comoving distance to redshift z is defined by

$$\frac{dr}{dz} = \frac{c}{H_0}\left[\Omega_k(1+z)^2 + \Omega_\Lambda + \Omega_M(1+z)^3 + \Omega_R(1+z)^4\right]^{-1/2} , \tag{15}$$

and integrating this equation over dz gives us $r(z)$.

To calculate the time since the big-bang we integrate the following,

$$dt = \frac{da}{a\,H_0}\left[\Omega_k a^{-2} + \Omega_\Lambda + \Omega_M a^{-3} + \Omega_R a^{-4}\right]^{-1/2} , \tag{16}$$

yielding an expression for $t(z)$. For our best-fit universe, there is an analytic expression for $t(z)$, which is

$$H_0 t(z) = \frac{2}{3\Omega_\Lambda^{1/2}} \sinh^{-1}\left[\left(\frac{\Omega_\Lambda}{\Omega_M}\right)^{1/2} (1+z)^{-3/2}\right] , \tag{17}$$

but there is no analytic expression for $r(z)$.

4.4. Observable Quantities

From these quantities we could naively calculate peak fluxes and fluences.

$$F_E^{\mathrm{P}} = \frac{L_{iso}^E}{4\pi r^2(z)(1+z)^2} = [\mathrm{erg\ s^{-1}\ cm^{-2}}] \qquad \mathrm{S_E} = \mathrm{F_E^P} \cdot \mathrm{T} \cdot (1+\mathrm{z}) = [\mathrm{erg\ cm^{-2}}] \tag{18}$$

$$F_N^{\mathrm{P}} = \frac{L_{iso}^N}{4\pi r^2(z)(1+z)} = [\mathrm{phot\ s^{-1}\ cm^{-2}}] \qquad \mathrm{S_N} = \mathrm{F_N^P} \cdot \mathrm{T} \cdot (1+\mathrm{z}) = [\mathrm{phot\ cm^{-2}}] \tag{19}$$

However, these are bolometric quantities, not observed quantities; in order to calculate the observed peak fluxes and fluences, we must model the detector.

We assume that the GRBs have a Band spectrum specified by $\alpha = -1$, $\beta = -2.5$ and $E_{\rm peak}^{\rm obs} = E_{\rm peak}/(1+z)$. We have also done simulations with $\alpha = -0.5$ and -1.5, and $\beta = -2.0$ and -3.0. These choices make little difference in our results.

Given $E_{\rm iso}$, $E_{\rm peak}$, and z from the simulations, we can calculate the normalization constant A^* by considering the bolometric fluence as observed in our reference frame.

$$S_E^{bol} = \frac{E_{\rm iso}}{4\pi(1+z)r(z)^2} = A^* \times \int_0^\infty EN(E;\alpha,\beta,E_{\rm peak}^{\rm obs},A=1)\,dE \tag{20}$$

Once we have A^*, we can calculate the observed fluxes and fluences in the passband of our instrument,

$$S_E^{obs} = \int_{instr} EN(E;\alpha,\beta,E_{\rm peak}^{\rm obs},A^*)\,dE \qquad F_E^{P,obs} = \frac{S_E^{obs}}{T(1+z)} \tag{21}$$

$$S_N^{obs} = \int_{instr} N(E;\alpha,\beta,E_{\rm peak}^{\rm obs},A^*)\,dE. \qquad F_N^{P,obs} = \frac{S_N^{obs}}{T(1+z)}. \tag{22}$$

To determine whether a particular burst will be detected by a particular instrument, we define the efficiency as a function of $E_{\rm peak}^{\rm obs}$,

$$\epsilon(E_{\rm peak}^{\rm obs}) = \frac{\int_{instr} N(E;\alpha,\beta,E_{\rm peak}^{\rm obs},A^*)\,dE}{\int_{0.1}^{10000} N(E;\alpha,\beta,E_{\rm peak}^{\rm obs},A^*)\,dE} = \frac{F_N^{P,inst}}{F_N^{P,\oplus}}. \tag{23}$$

This expression gives a shape function which we normalize to Figures 2 through 9 of Band (2003) for the desired detector. Note that our shape function is the same as Band's, except that we consider incident burst spectra extending from 0.1 - 10,000 keV instead of from 1 - 1000 keV, in order to encompass the full range of values of $E_{\rm peak}^{\rm obs}$ that may occur.

This normalization we use is approximately given by

$$D_{inst} = \frac{C_{min}(\sigma, B)}{A_{eff} \cdot \Delta t_{trig}} = [\text{phot s}^{-1}\ \text{cm}^{-2}]. \tag{24}$$

A burst is detected if

$$F_N^{P,\oplus} \geq \frac{D_{\rm inst}}{\epsilon(E_{\rm peak}^{\rm obs})} = F_{N,min}^{P,\oplus} \qquad F_N^{P,\rm inst} \geq D_{\rm inst} = F_{N,min}^{P,\rm inst}. \tag{25}$$

Thus D_{inst} is the peak number flux detection threshold in the instrument passband.

We reproduce the results of Band (2003) for BATSE on CGRO, the WFC and GRBM on *Beppo*SAX , and the WXM and FREGATE on *HETE-2* . Figure 7 shows the threshold sensitivity curves in peak photon number flux $F_N^{\rm P}$ for the WXM and FREGATE on HETE-2 and for the WFC and GRBM on *Beppo*SAX as a function of $E_{\rm peak}^{\rm obs}$, the observed peak energy of the burst νF_ν spectrum. Since, *Beppo*SAX could not trigger on WFC data and was forced to rely on the less-sensitive GRBM for its triggers, we consider a burst to have been detected by *Beppo*SAX only if its peak flux falls above the GRBM sensitivity threshold. Since *HETE-2* can trigger on WXM data, we consider a burst to have been detected if its peak flux falls above the minimum of the WXM and FREGATE sensitivity thresholds. These bursts form the ensemble of observed bursts from which we construct various observed distributions.

5. Results

To test our uniform jet model against the structured jet model, we consider two possibilities. In one case, we require the structured jet model to account for the full range of the Amati relation; that is, we adjust the normalization of E_γ^0 to constrain the lowest $E_{\rm iso}$ allowed in the model to the value obtained for XRF 020903. In the other case, we constrain the lowest allowed $E_{\rm iso}$ to the value obtained for GRB 980326, the faintest GRB in the *Beppo*SAX sample.

Figure 9 shows scatter plots of S_N (upper row) and S_E (lower row) versus $\Omega_{\rm jet}$. The left column is the uniform jet model, while the right column is universal jet model pinned to XRF 020903.

Figure 10 shows scatter plots of $F_N^{\rm P}$ (left column) and $F_E^{\rm P}$ (right column) versus $\Omega_{\rm jet}$. The upper row is the uniform jet model, the middle row is the universal jet model pinned to XRF 020903 and bottom row is the universal jet model pinned to GRB 980326.

Figure 11 shows the cumulative distribution of $\Omega_{\rm jet}$ values for bursts detected in various models. The left-hand panel shows the uniform jet model for $\delta_{sim} = 0$, 1 and 2. The right-hand panel shows the universal jet model pinned to XRF 020903 (solid red line) and pinned to GRB 980326 (dashed red line). The solid black histogram shows the observed distribution of $\Omega_{\rm jet}$ (Bloom, Frail & Kulkarni 2003), scaled by a factor of $C_{jet} = 95.5$.

Figure 12 shows scatter plots comparing the predictions of the three models with the observed distribution of bursts. The left column shows scatter plots of E_{iso} vs. E_p with observed bursts from *HETE-2* and *Beppo*SAX with known redshift. The right column shows scatter plots of E_p^{obs} vs. $S_E(2-400keV)$ with a larger set of observed bursts from *HETE-2* . The top row is the uniform jet model, the middle row is the universal jet model pinned to XRF 020903 and the bottom row is the universal jet model pinned to GRB 980326.

Figure 13 shows cumulative distributions of four observable quantities and compares the three models against the same datasets as above. In each case, the blue curve is the uniform jet model, the solid red curve is the universal jet model pinned to XRF 020903 and the dashed red curve is the universal jet model pinned to GRB 980326.

Figure 14 shows scatter plots of $1+z$ vs. $F_N^{\rm P}$ (left column) and $E_{\rm peak}^{\rm obs}$ (right column). The top row is uniform jet model, the middle row is the universal jet model pinned to XRF 020903 and the bottom row is the universal jet model pinned to GRB 980326. The points represent *HETE-2* bursts with known redshift.

Figure 15 shows scatter plots of the three models in the L_γ vs. E_p plane. The upper figures depict the universal jet model pinned to XRF 020903 (left) and GRB 980326 (right). Lower left figure is the same for the uniform jet model. Lower right compares the cumulative distributions of the three models against the *HETE-2* data points.

Figure 16 shows the cumulative and differential distributions in $F_E^{\rm P}$. The left-hand panel compares the cumulative distributions of $F_E^{\rm P}$ for the three models. The right-hand panel shows the differential distribution of $E_{\rm peak}^{\rm obs}$ in the uniform jet model for cuts at $F_E^P = 10^{-6}$, 10^{-7} and 10^{-8} erg cm^{-2} s^{-1}.

Figure 17 shows the cumulative (left) and differential (right) distributions of GRBs detected by HETE-2 in $1+z$ for the three models.

6. Discussion

As we have seen, HETE-2 has provided strong evidence that the properties of XRFs, X-ray-rich GRBs, and GRBs form a continuum, and that these bursts are therefore the same phenomenon. If this is true, it immediately implies that the E_γ inferred by Frail et al. (2001) is too large by a factor of at least 100 (Lamb et al. 2003). The reason is that the values of $E_{\rm iso}$ for XRF 020903 (Sakamoto et al. 2003a) and XRF 030723 (Lamb et al. 2003) are ~ 100

times smaller than the value of E_γ inferred by Frail et al. – an impossibility.

HETE-2 has also provided strong evidence that, in going from XRFs to GRBs, $E_{\rm iso}$ changes by a factor $\sim 10^5$ (see Figure 2). Figures 10 - 18 show that, if one tries to explain only the range in $E_{\rm iso}$ corresponding to GRBs, both the uniform jet model and the structured jet model work reasonably well. However, if one tries to explain the range in $E_{\rm iso}$ of a factor $\sim 10^5$ that is required in order to accommodate both XRFs and GRBs in a unified description, the uniform jet works reasonably well while the structured jet model fails utterly.

The reason is the following: the observational implications of the universal jet model and the uniform jet model differ dramatically if they are required to explain XRFs and GRBs in a unified picture. In the universal jet model, most viewing angles θ_v are $\approx 90°$. This implies that the number of XRFs should exceed the number of GRBs by many orders of magnitude, something that HETE-2 does not observe (see Figures 1, 2, 4, and 5). On the other hand, by choosing $N(\Omega_{\rm jet}) \sim \Omega_{\rm jet}^{-2}$, the uniform jet model predicts equal numbers of bursts per logarithmic decade in $E_{\rm iso}$ (and S_E), which is exactly what HETE-2 sees (again, see Figures 1, 2, 4, and 5) (Lamb et al. 2003).

Thus, if $E_{\rm iso}$ spans a range $\sim 10^5$, as the HETE-2 results strongly suggest, the uniform jet model can provide a unified picture of both XRFs and GRBs, whereas the universal jet model cannot. This means that XRFs provide a powerful probe of GRB jet structure.

6.1. Rate of GRBs and the Nature of Type Ic Supernovae

A range in $E_{\rm iso}$ of 10^5, which is what the HETE-2 results strongly suggest, requires a *minimum* range in $\Delta\Omega_{\rm jet}$ of $10^4 - 10^5$ in the uniform jet model. Thus the unified picture of XRFs and GRBs in the uniform jet model implies that there are $\sim 10^4 - 10^5$ more bursts with very small $\Omega_{\rm jet}$'s for every such burst we see; i.e., the rate of GRBs may be ~ 100 times greater than has been thought.

In addition, since the observed ratio of the rate of Type Ic SNe to the rate of GRBs in the observable universe is $R_{\rm Type\ Ic}/R_{\rm GRB} \sim 10^5$ (Lamb 1999), the unified jet model implies that roughly *all* Type Ic SNe produce high-energy transients. More spherically symmetric jets yield XRFs and narrow jets produce GRBs. Then low $E_{\rm peak}$ (intrinsically faint) XRFs likely probe core collapse supernovae that produce wide jets, while high $E_{\rm peak}$ (intrinsically luminous) GRBs likely probe core collapse supernovae that produce very narrow jets.

Thus XRFs and GRBs may provide a combination of GRB/SN samples that would enable astronomers to study the relationship between the degree of jet-like behavior of the

GRB and the properties of the supernova (brightness, polarization $\Leftrightarrow$ asphericity of the explosion, velocity of the explosion $\Leftrightarrow$ kinetic energy of the explosion, etc.). GRBs may therefore provide a unique laboratory for understanding Type Ic core collapse supernovae.

A unified picture of XRFs and GRBs in the uniform jet model also implies that most Type Ic SNe produce narrow jets, which may suggest that the collapsing cores of most Type Ic supernovae are rapidly rotating. Finally, as we have seen, such a unified picture implies that the total radiated energy in gamma rays E_γ is $\sim$ 100 times smaller than has been thought.

6.2. Detection of GRBs by Gravitational Wave Detectors

If as the unified jet model implies, most GRBs are bright and have narrow jets – possibly implying that the collapsing core of the progenitor star may be rapidly rotating – GRBs might be detectable sources of gravitational waves. If as has been argued, $E_{\rm gw}/E_{\rm rot} \sim 5\%$ in the formation of a black hole from the collapse of the core of the Type Ic supernova (van Putten & Levinson 2002), where $E_{\rm gw}$ is the energy emitted in gravitational waves and $E_{\rm rot}$ is the rotational energy of the newly formed black hole, and the rate of GRBs is $\sim$ 100 times higher than has been thought, then the rate of LIGO/VIRGO detections of GRBs would be about 5 yr^{-1} rather than about 1 yr^{-1} van Putten & Levinson (2002).

6.3. Other Observations That Favor the Unified Jet Model

6.3.1. Polarization of GRBs and Their Afterglows

Part of the motivation for the universal jet model comes from the expectation that in hydrodynamic jets, entrainment and the interaction of the ultra-relativistic outflow with the core of the progenitor star may well result in a strong fall-off of the velocity of the flow away from the jet axis. The narrow jets we find are favored in the unified picture of XRFs and GRBs based on the uniform jet model are difficult to reconcile with hydrodynamic jets, which strongly suggests that GRB jets are magnetic-energy dominated; i.e., GRBs come from MHD jets. Such jets can be quite narrow Vlakakis & Königl (2001) and may resist the entrainment material from the core of the progenitor star. This possibility has received additional support from the recent discovery that GRB 021206 was strongly polarized (Coburn & Boggs 2003).

Zhang & Mészáros (2003) and Kumar & Panaitescu (2003) have studied the early afterglows of two GRB. Zhang & Mészáros (2003) find in the case of GRB 990123 strong evidence that the jet is magnetic energy dominated; Kumar & Panaitescu (2003) reach a similar conclusion for GRB 021211. In both cases, it appears that the magnetic energy dominated the kinetic energy in the ejected matter by a factor > 1000. These results provide further support for the picture that GRBs come from magnetic-energy dominated jets.

Another discriminant between the uniform jet model and the universal jet model is the behavior of the polarization of the optical afterglow. The uniform jet model predicts that the polarization angle should change by 180○ over time, passing through 0 around the time of the jet break in the afterglow light curve. In contrast, the universal jet model predicts that the polarization angle should not change with time. The polarization data on GRB afterglows that has been obtained to date is typically very sparse, making it difficult to tell whether or not the behavior of the polarization favors the uniform or the universal jet model.

In the case of GRB 021004, however, there is clear evidence that the polarization angle changed by approximately 180○ and changed sign around the time of the jet break, as the uniform jet model but not the universal jet model predicts Rol et al. (2003). Thus, in the case of this one GRB, at least, the uniform jet model is strongly favored over the universal jet model.

6.3.2. Global modeling of GRB afterglows

Panaitescu & Kumar (2003) have carried out global modeling of two GRB afterglows. In both cases, they find that fits to the X-ray, optical, NIR, and radio data for GRBs 990510 and 000301c favor the uniform jet model over the universal jet model.

6.4. Observations That May Disfavor the Unified Jet Model

We now discuss observations that may disfavor the unified picture of XRFs, X-ray-rich GRBs, and GRBs based on the uniform jet model.

XRFs 020903 and 030723 lie squarely on the relation between $E_{\rm iso}$ and $E_{\rm peak}$ found by Amati et al. (2002) (see Figure 2). However, the implied values of E_γ from the break times are much smaller (a factor ~ 100 smaller in the case of XRF 020903) than the "standard energy" of $E_\gamma = 1.3 \times 10^{49}$ that we find in this work and a factor $\sim 10^4$ smaller than the "standard energy" of $E_\gamma = 1.3 \times 10^{49}$ found by Bloom, Frail & Kulkarni (2003) (see also Frail et al. (2001)).

While there is substantial uncertainty in the jet opening angle implied by the jet break time (Rhoads 1999; Sari & Piran & Halpern 1999), the global modeling of GRB afterglows is largely free from this uncertainty. Such modeling tends to find jet opening angles $\sim$ a few degrees for the brightest and hardest GRBs – which is a factor of at least 3, and perhaps a factor of 10, larger than the jet opening angles we find in this work.

Berger et al. (2003() have monitored the late-time radio emission of a sample of 33 nearby Type Ic supernovae. They find that, in most cases, the energy emitted at radio wavelengths $E_{\rm radio} < 10^{48}$ ergs for most Type Ic supernovae. This implies that these supernovae do not produce jets with energies $E_{\rm jet} > 10^{48}$ ergs, and therefore that, at most $\sim 10\%$ of all Type Ic supernovae produce GRBs. While not directly contradicting our unified jet picture of XRFs and GRBs, these radio observations place an important constraint on them.

6.5. Testing the Unified Jet Model

As we have seen, the HETE-2 results provide strong evidence that XRFs and GRBs are the same phenomenon. But the profound implications of these results in terms of the structure of GRB jets, the rate of GRBs, and the nature of Type Ic supernovae, require incontrovertible evidence.

Obtaining the incontrovertible evidence needed to confirm (or rule out) the unified jet picture of XRFs, X-ray-rich GRBs, and GRBs, based on the uniform jet model, and the profound implications implications for the structure of GRB jets, the GRB rate, and Type Ic supernovae, will require accurate, rapid localizations of XRFs, leading to identification of their X-ray and optical afterglows and the determination of their redshifts. Until very recently, only one XRF (XRF 020903; Soderberg et al. 2002) had even a probable optical afterglow and redshift (see Figure 18). The reason why is that, as expected in the uniform jet picture, the X-ray (and therefore the optical) afterglows of XRFs are $\sim 10^3 - 10^4$ times fainter than those of GRBs (see Figure 19). But this challenge can be met: the recent HETE-2–localization of XRF 030723 represents the first time that an XRF has been localized in real time (Prigozhin et al. 2003); identification of its X-ray and optical afterglows rapidly followed (Fox et al. 2003). This event may well be the Rosetta stone for XRFs.

The exciting recent results involving XRF 030723 highlight the fact that HETE-2 can obtain the evidence about XRFs that is required to confirm or rule out the unified jet model and the profound implications about the structure of GRB jets, the rate of GRBs, and the nature of Type Ic supernovae that it implies whereas *Swift* will not. This is demonstrated in Figure 20 shows the ratio of the rate of detection by WXM on *HETE-2* and BAT on *Swift* of XRFs with peak energies less than $E_{\rm peak}$ in the unified jet model. This figure shows that the SXC and WXM instruments on HETE-2 detect XRFs with peak energies $E_p^{\rm obs} < 5$ keV at *10 times* the rate that BAT on *Swift* can be expected to have. *Swift* will therefore detect very few such XRFs. Specifically, HETE-2 has localized 17 XRFs in 2 1/2 years; *Swift* can therefore be expected to localize ~ 1 XRF with $E_p^{\rm obs} < 5$ keV during its 2-year prime mission. HETE-2's ability to accurately and rapidly localize XRFs – and study their spectra – therefore constitutes a compelling reason for continuing HETE-2 during the *Swift* mission.

7. Conclusions

In this paper, we have shown that a uniform jet model, in which the isotropic-equivalent energy depends on the solid angle $\Omega_{\rm jet}$, can account for the observed properties of all three types of GRBs in a unified way. In contrast, we show that, although the universal jet model can account for the observed properties of GRBs, it cannot easily accommodate the properties of the other types of GRBs. According to the unified (uniform) jet model, most bursts have very small values of $\Omega_{\rm jet}$. These are the hardest and most luminous bursts; however, we see a very small fraction of them. HETE-2 observations show that $E_{\rm iso}$, the isotropic-equivalent radiated energy of GRBs, spans five decades, implying a *minimum* range $\Delta\Omega_{\rm jet} \sim 10^5$. The unified jet model therefore implies that there are $\sim 10^5$ more bursts with very small $\Omega_{\rm jet}$'s for every such burst we see. The observed ratio of the rate of Type Ib/Ic supernovae to the rate of GRBs in the observable universe is $R_{\rm Type Ib/Ic}/R_{\rm GRB} \sim 10^5$, and therefore the unified model implies that roughly *all* Type Ib/Ic supernovae produce high-energy transients, with spherically symmetric jets yielding XRFs and narrow jets producing GRBs. Thus GRBs may be a crucial laboratory for understanding Type Ib/Ic core collapse supernovae. In particular, the unified jet model implies that most Type Ib/Ic supernovae produce narrow jets, which may suggest that the collapsing cores of most Type Ib/Ic supernovae are rapidly rotating. The unified model also implies that the total radiated energy in gamma rays E_γ is ~ 100 times smaller than has been thought, and the efficiency of conversion of the kinetic energy of the jet $E_{\rm jet}$ into radiation is only ~ 2 %, a much easier task for the internal shock model to achieve. The model implies that the hardest and most brilliant GRBs have jet solid angles $\Omega_{\rm jet}/2\pi \sim 10^{-5}$. Such small solid angles are difficult to achieve with hydrodynamic jets, which suggests that GRB jets are magnetically dominated.

This research was supported in part by NASA Contract NAGW-4690 and NASA Grant NAG5-10759.

REFERENCES

Amati, L., et al. 2002, A&A, 390, 81

Atteia, J-L, et al. 2003, in Gamma-Ray Burst and Afterglow Astronomy 2001, AIP Conf. Proceedings 662, ed. G. R. Ricker & R. K. Vanderspek (New York: AIP), 17

Band, D. L. 2003, ApJ, in press (astro-ph/0212452)

Berger, E., Kulkarni, S. R., Frail, D. A., & Soderberg, A. M. 2003, ApJ, submitted (astro-ph/0307228)

Bloom, J., Frail, D. A. & Kulkarni, S. R. 2003, ApJ, 588, 945

Coburn, W. & Boggs, S. E. 2003, Nature, 423, 415

Dermer, C. D., Chiang, J., & Böttcher, M. 1999a, ApJ, 513, 656

Dermer, C. D. 1999b, in AIP Conf. Proc. 526, ed. R M. Kippen, R. S. Mallozzi, G. J. Fishman (New York: AIP), 435

Fox, D. W., et al. 2003, GCN Circular 2323

Frail, D. et al. 2001, ApJ, 562, L55

Heise, J., in't Zand, J., Kippen, R. M., & Woods, P. M., in Proc. 2nd Rome Workshop: Gamma-Ray Bursts in the Afterglow Era, eds. E. Costa, F. Frontera, J. Hjorth (Berlin: Springer-Verlag), 16

Huang, Y. F., Dai, Z. G. & Lu, T. 2002, MNRAS, 332, 735

Kawai, N., et al. 2003, in Gamma-Ray Burst and Afterglow Astronomy 2001, AIP Conf. Proceedings 662, ed. G. R. Ricker & R. K. Vanderspek (New York: AIP), 25

Kippen, R. M., Woods, P. M., Heise, J., in't Zand, J., Briggs, M.S., & Preece, R. D. 2002, in Gamma-Ray Burst and Afterglow Astronomy, AIP Conf. Proceedings 662, ed. G. R. Ricker & R. K. Vanderspek (New York: AIP), 244

Kumar, P., & Panaitescu, A. 2003, ApJ, submitted (astro-ph/0305446)

Lamb, D. Q. 1999, A&A, 138, 607

Lamb, D. Q. 2000, Physics Reports, 333-334, 505

Lamb, D. Q., et al. 2003, ApJ, submitted

Lloyd-Ronning, N., Petrosian, V., & Mallozzi, R. S. 2000, ApJ, 534, 227

Mészáros, P., Ramirez-Ruiz, E., Rees, M. J., & Zhang, B. 2002, ApJ, 578, 812

Mochkovitch, R., Daigne, F., Barraud, C., & Atteia, J. L. 2003, ASP Conference Series (San Francisco: ASP), in press (astro-ph/0303289)

Panaitescu, A. & Kumar, P. 2003, ApJ, submitted (astro-ph/0301032)

Prigozhin, G., et al. 2003, GCN Circular 2313

van Putten, M. H. P. M., & Levinson, A. 2002, Class. Quantum Grav., 19, 1309

Ramirez-Ruiz, E. & Lloyd-Ronning, N. 2002, New Astronomy, 7, 197

Rhoads, J. E. 1999, ApJ, 525, 737

Ricker, G. R. et al. 2003, in Gamma-Ray Burst and Afterglow Astronomy 2001, AIP Conf. Proceedings 662, ed. G. R. Ricker & R. K. Vanderspek (New York: AIP), 3

Ricker, G. R. et al. 2003, in preparation

Rol, E., et al. 2003, A&A, 405, L23

Rossi, E., Lazzati, D, & Rees, M. J. 2002, MNRAS 332, 945

Rowan-Robinson, M. 2001, ApJ, 549, 745

Sakamoto, T. et al. 2003a, ApJ, submitted

Sakamoto, T. et al. 2003b, ApJ, to be submitted

Sari, R., Piran, T., & Halpern, J. P. 1999, ApJ, 519, L17

Vlahakis, N., & Königl, A. 2001, ApJ, 563, L129

Woosley, S. E., Zhang, W. & Heger, A. 2003, ApJ, submitted (astro-ph/0206004)

Yamazaki, R., Ioka K. & Nakamura T. 2002, ApJ, 571, L31

Yamazaki, R., Ioka K. & Nakamura T. 2003, ApJ, submitted (astro-ph/0212557)

Zhang, B. & Mészáros, P. 2002, ApJ, 571, 876

Zhang & Mészáros, P. 2003, ApJ, in press (astro-ph/0206158)

This preprint was prepared with the AAS LATEX macros v5.0.

Table 1. Gaussian Smearing Functions

Quantity	Central Value[a]	Sigma[a]	Source
Jet Energy – E_γ [erg]	51.124	0.35	Bloom et al., 2003
Amati Coefficient – C [keV]	1.950	0.13	Amati et al., 2002; Lamb et al., 2003
Timescale – T [sec]	0.574	0.305	Amati et al., 2002; Lamb et al., 2003

[a]Log-normal distribution.

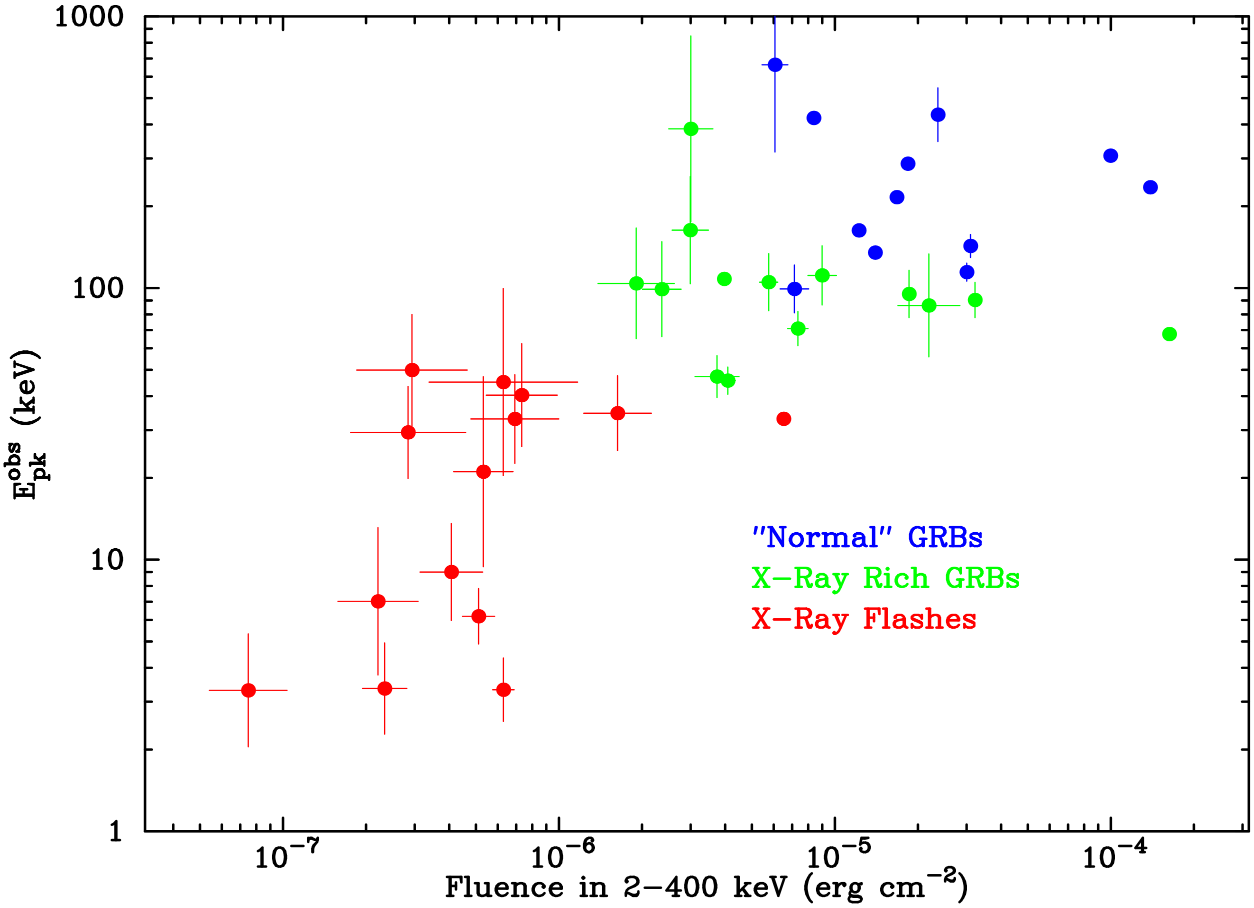

Fig. 1.— Distribution of HETE-2 bursts in the $[S(2-400\mathrm{keV}), E^{\mathrm{obs}}_{\mathrm{peak}}]$-plane, showing XRFs (red), X-ray-rich GRBs (green), and GRBs (blue). This figure shows that XRFs and X-ray-rich GRBs comprise about 2/3 of the bursts observed by *HETE-2* , and that the properties of the three kinds of bursts form a continuum. From Sakamoto et al. (2003b).

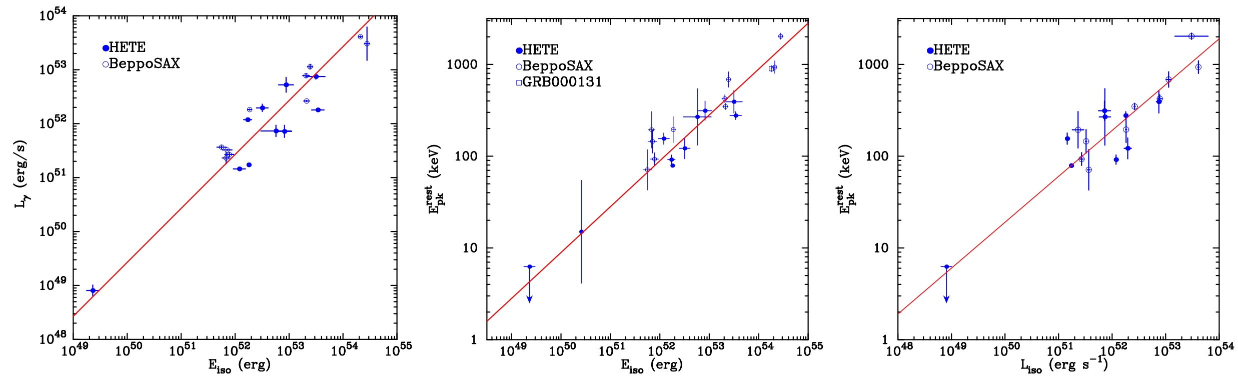

Fig. 2.— Left panel: distribution of HETE-2 and *Beppo*SAX bursts in the ($E_{\rm iso}$,L_γ)-plane, where $E_{\rm iso}$ and L_γ are the isotropic-equivalent GRB energy and luminosity in the source frame. Middle panel: distribution of HETE-2 and *Beppo*SAX bursts in the ($E_{\rm iso}$,$E_{\rm peak}$)-plane, where $E_{\rm peak}$ is the energy of the peak of the burst νF_ν spectrum in the source frame. The HETE-2 bursts confirm the relation between $E_{\rm iso}$ and $E_{\rm peak}$ found by Amati et al. (2002), and extend it by a factor ~ 300 in $E_{\rm iso}$. Right panel: distribution of HETE-2 and *Beppo*SAX bursts in the (L_γ,$E_{\rm peak}$)-plane. The distribution of HETE-2 and *Beppo*SAX bursts in the three planes demonstrates that there is a linear relation between $\log E_{\rm iso}$ and $\log L_\gamma$ that extends over at least five decades in both quantities, and are linear relations between both $\log E_{\rm iso}$ and $\log L_\gamma$ and $log E_{\rm peak}$ that extends over at least 2.5 decades in $E_{\rm peak}$. The bursts with the lowest and second-lowest values of $E_{\rm iso}$ and L_γ are XRFs 020903 and 030723. The first relation is implied by the "standard energy" for GRBs found by Frail et al. (2001). From Lamb et al. (2003).

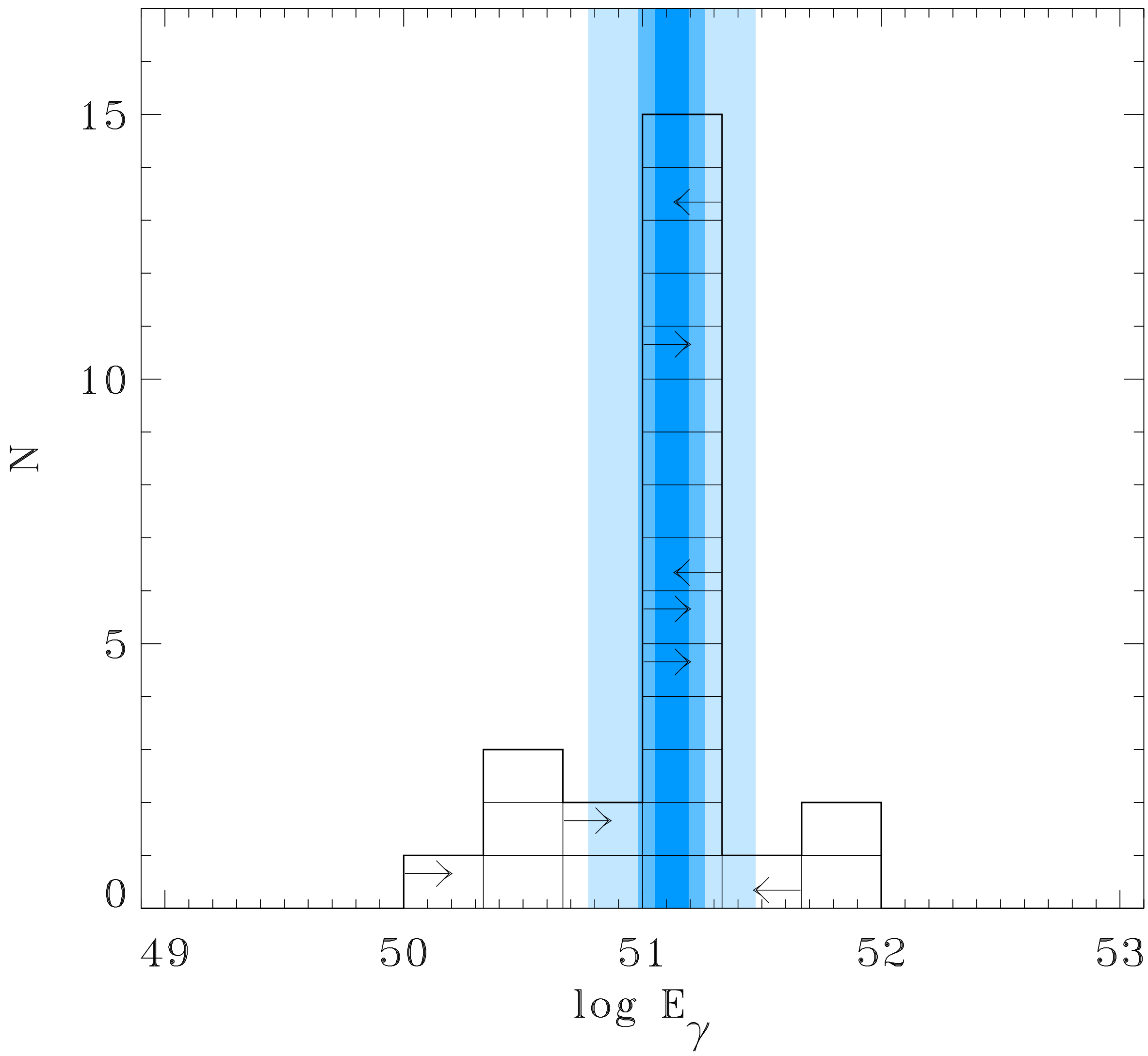

Fig. 3.— Distribution of isotropic-equivalent energies $E_{\rm iso}$ ($E_{\rm iso}$) (top panel) and resulting distribution of total radiated energy in gamma-rays, taking into account the jet opening angle inferred from the jet break time (bottom panel). From Bloom, Frail & Kulkarni (2003).

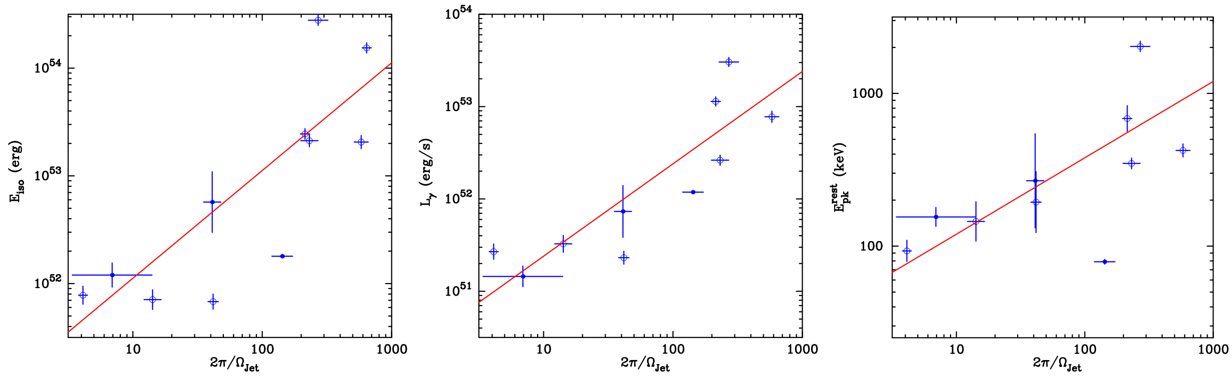

Fig. 4.— Left panel: distribution of HETE-2 and *Beppo*SAX bursts in the $(2\pi/\Omega_{\rm jet},E_{\rm iso})$-plane, where $E_{\rm iso}$ is the isotropic-equivalent burst energy in the source frame. In the uniform jet model, $\Omega_{\rm jet}$ is the jet solid angle; in the universal jet model it is the solid angle interior to the viewing angle $\theta_{\rm view}$. Middle panel: distribution of HETE-2 and *Beppo*SAX bursts in the $(2\pi/\Omega_{\rm jet},L_\gamma)$-plane, where L_γ is the isotropic-equivalent burst luminosity in the source frame. Right panel: distribution of HETE-2 and *Beppo*SAX bursts in the $(2\pi/\Omega_{\rm jet},E_{\rm peak})$-plane, where $E_{\rm peak}$ is the energy of the peak of the burst νF_ν spectrum in the source frame. The distribution of HETE-2 and *Beppo*SAX bursts in these three planes demonstrates that there are linear relations between both $\log E_{\rm iso}$ and $\log L_\gamma$ and $\log \Omega_{\rm jet}^{-1}$ that extends over at least 2.5 decades in $\log E_{\rm iso}$ and $\log L_\gamma$, and a relation of slope 1/2 between $\log E_{\rm peak}$ and $\log \Omega_{\rm jet}^{-1}$ that extends over at least 1.25 decades in $E_{\rm peak}$.

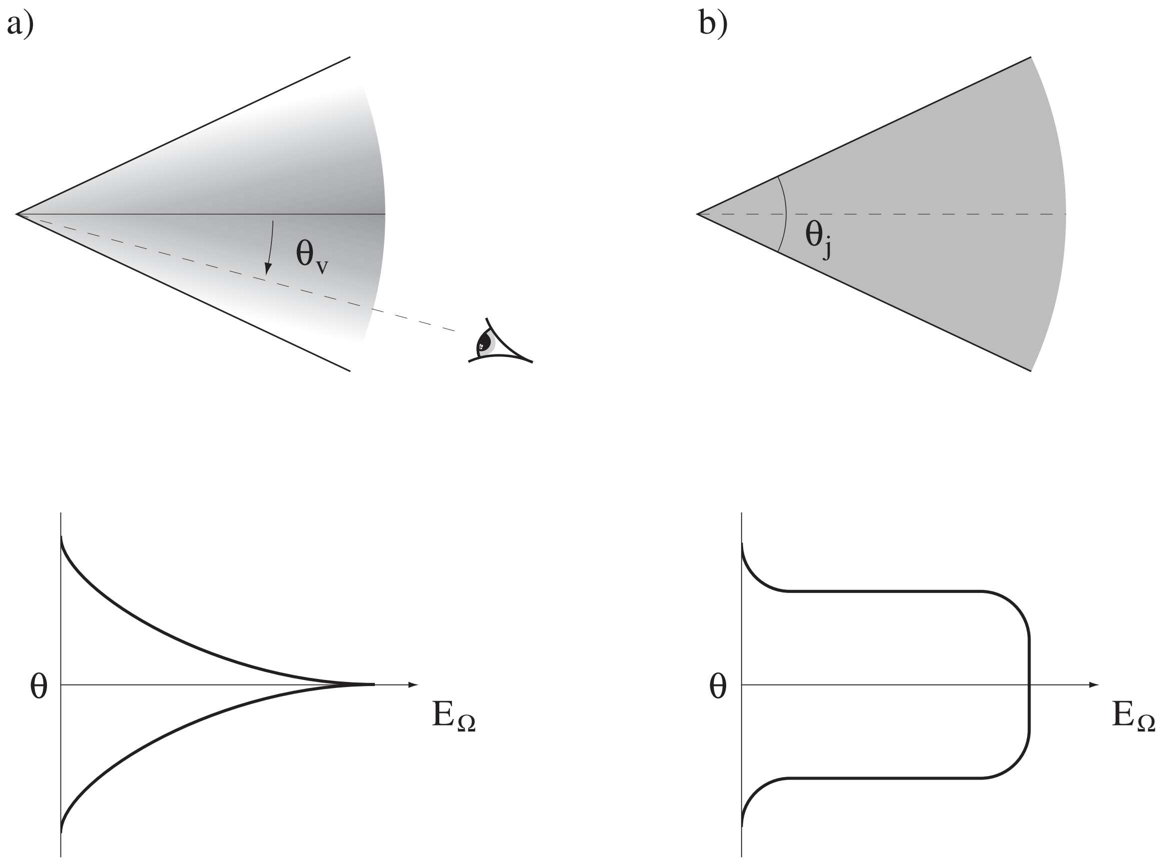

Fig. 5.— Schematic diagrams of universal and uniform jet models of GRBs from Ramirez-Ruiz & Lloyd-Ronning (2002). In the universal jet model, the isotropic-equivalent energy and luminosity is assumed to decrease as the viewing angle θ_v as measured from the jet axis increases. In order to recover the "standard energy" result (Frail et al. 2001), $E_{\rm iso}(\theta_v) \sim \theta_v^{-2}$ is required. In the uniform jet model, GRBs produce jets with a large range of jet opening angles $\theta_{\rm jet}$. For $\theta < \theta_{\rm jet}$, $E_{\rm iso}(\theta_v) =$ constant while for $\theta > \theta_{\rm jet}$, $E_{\rm iso}(\theta_v) = 0$.

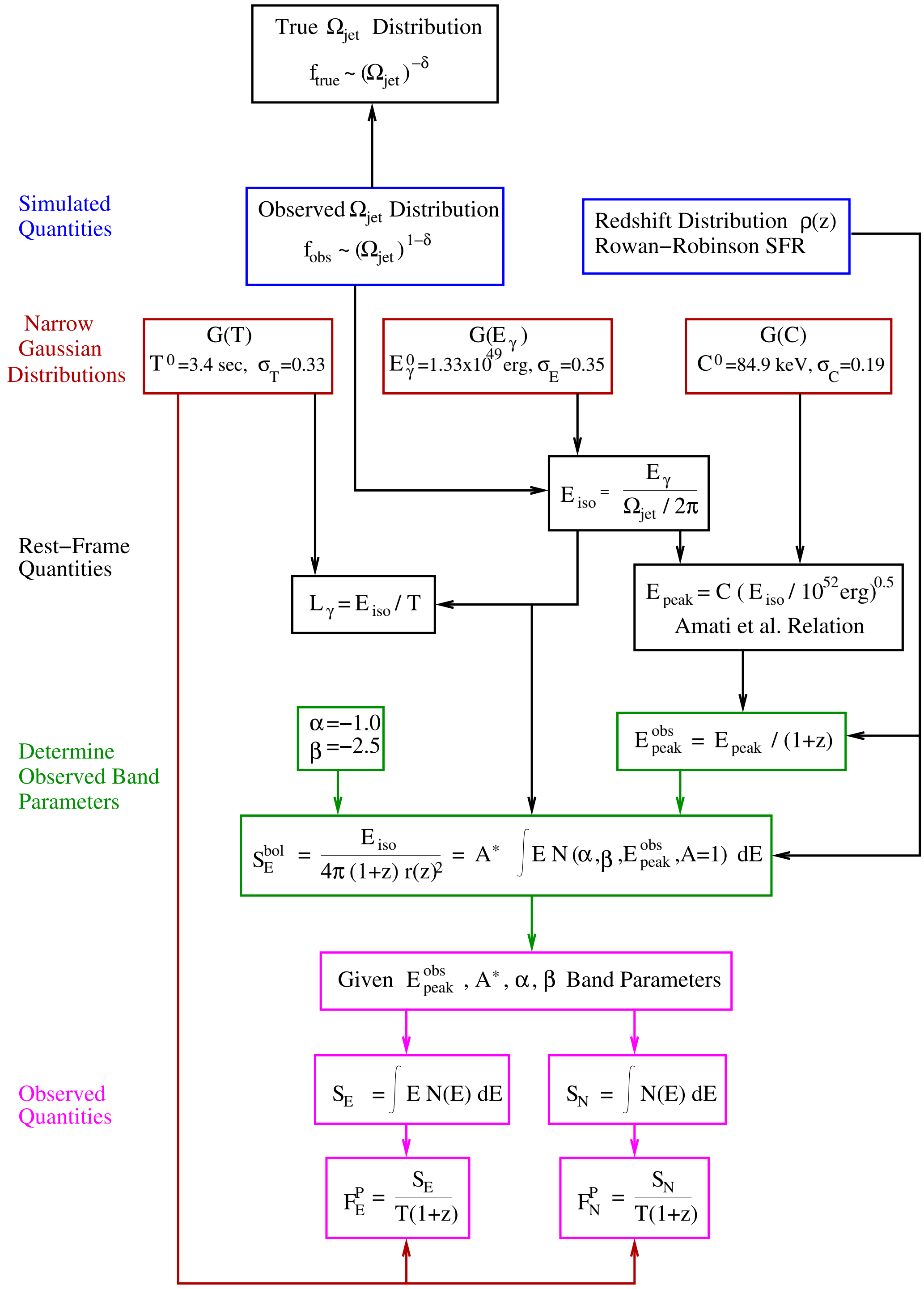

Fig. 6.— Flowchart showing the logical sequence of the jet-model simulations.

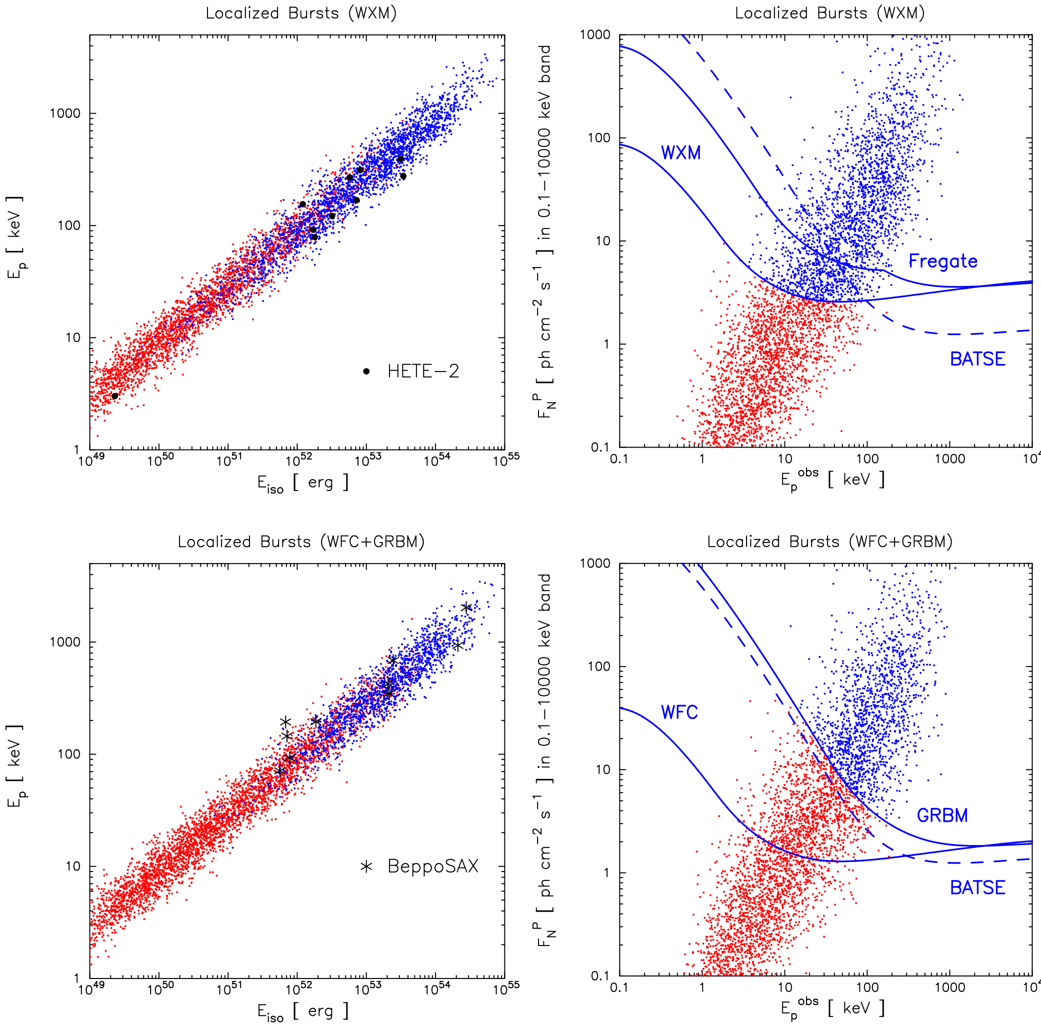

Fig. 7.— Comparison of the detectability of bursts in the uniform jet model by *HETE-2* and *Beppo*SAX . For each experiment, we over plot the actual observed data points. Detected bursts are shown in blue with non-detected bursts in red. The left-hand panels show bursts in the $[E_{\rm iso}, E_{\rm peak}]$-plane detected by *Beppo*SAX (upper) and *HETE-2* (lower). The right-hand panels show bursts in the $[E_{\rm peak}^{\rm obs}, F_N^{\rm P}(0.1 - 10000{\rm keV})]$-plane detected by *Beppo*SAX (upper) and *HETE-2* (lower). For each experiment we show the sensitivity thresholds for their respective instruments over plotted in solid blue. The BATSE threshold is shown in both figures as a dashed blue line.

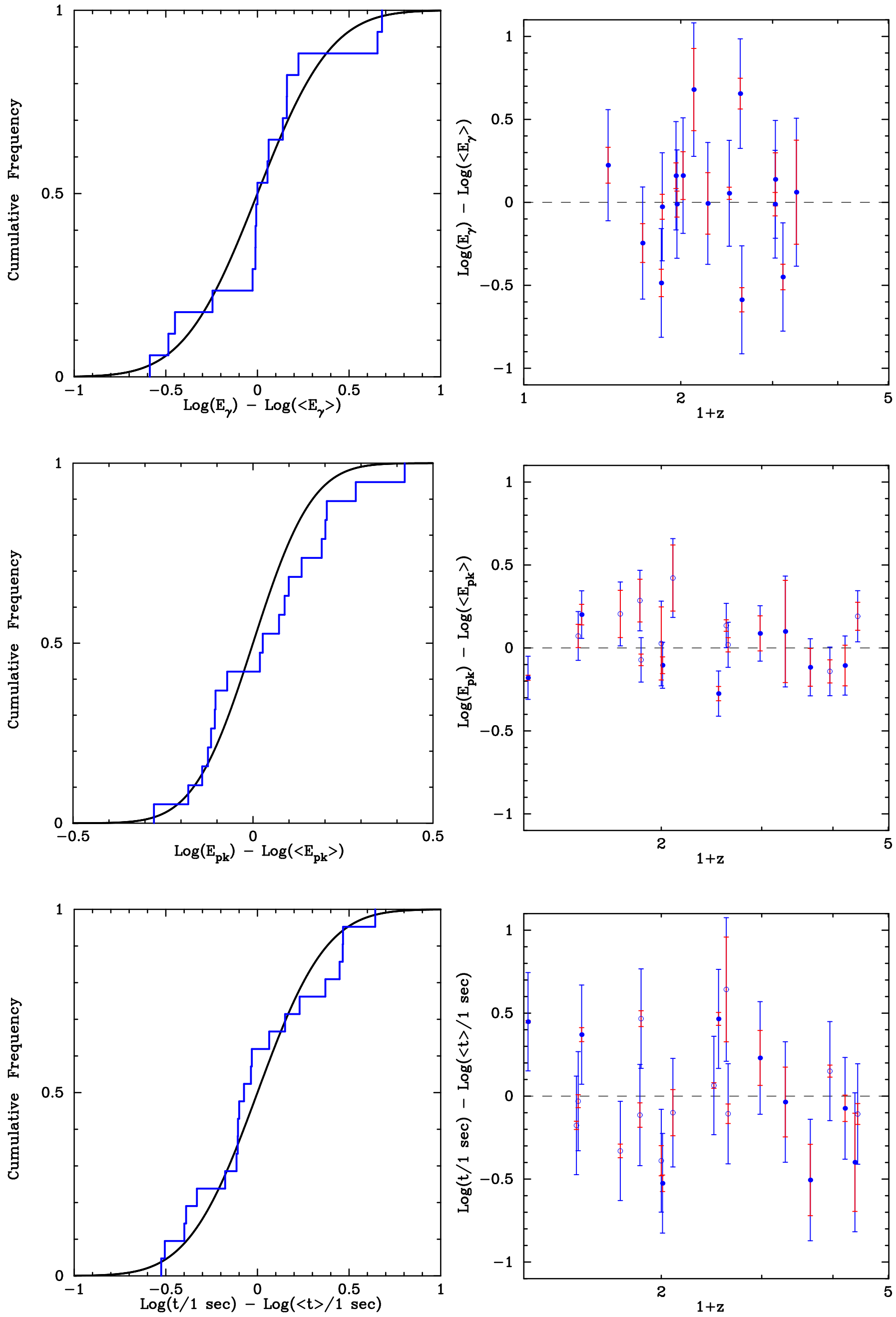

Fig. 8.— Left panels: E_γ (top), $T_0 \sim F_N^{\mathrm{P}}/S_E$ (middle), and the deviation ΔE_{peak} in E_{peak} of bursts from the $E_{\mathrm{iso}} - E_{\mathrm{peak}}$ relation that we have adopted (bottom), as a function of redshift z. Right panels: comparison of the best-fit smearing functions $G(E_\gamma)$, $G(T)$, and $G(C)$ and the cumulative distributions of E_γ (top), T_0 (middle), and ΔE_{peak} (bottom), respectively.

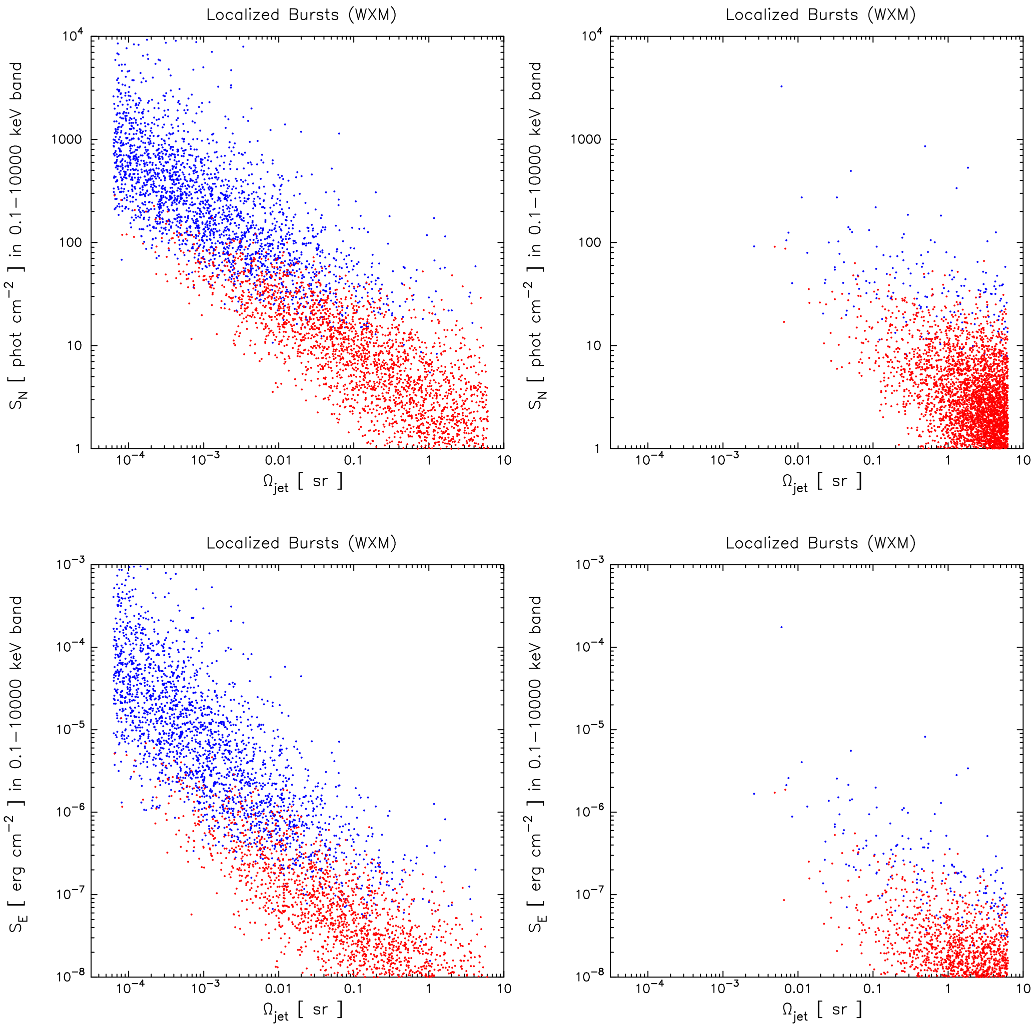

Fig. 9.— Scatter plots of S_E, S_N and F_E^P versus Ω_{jet}. Left column is uniform jet model, while right column is universal jet model pinned to XRF 020903.

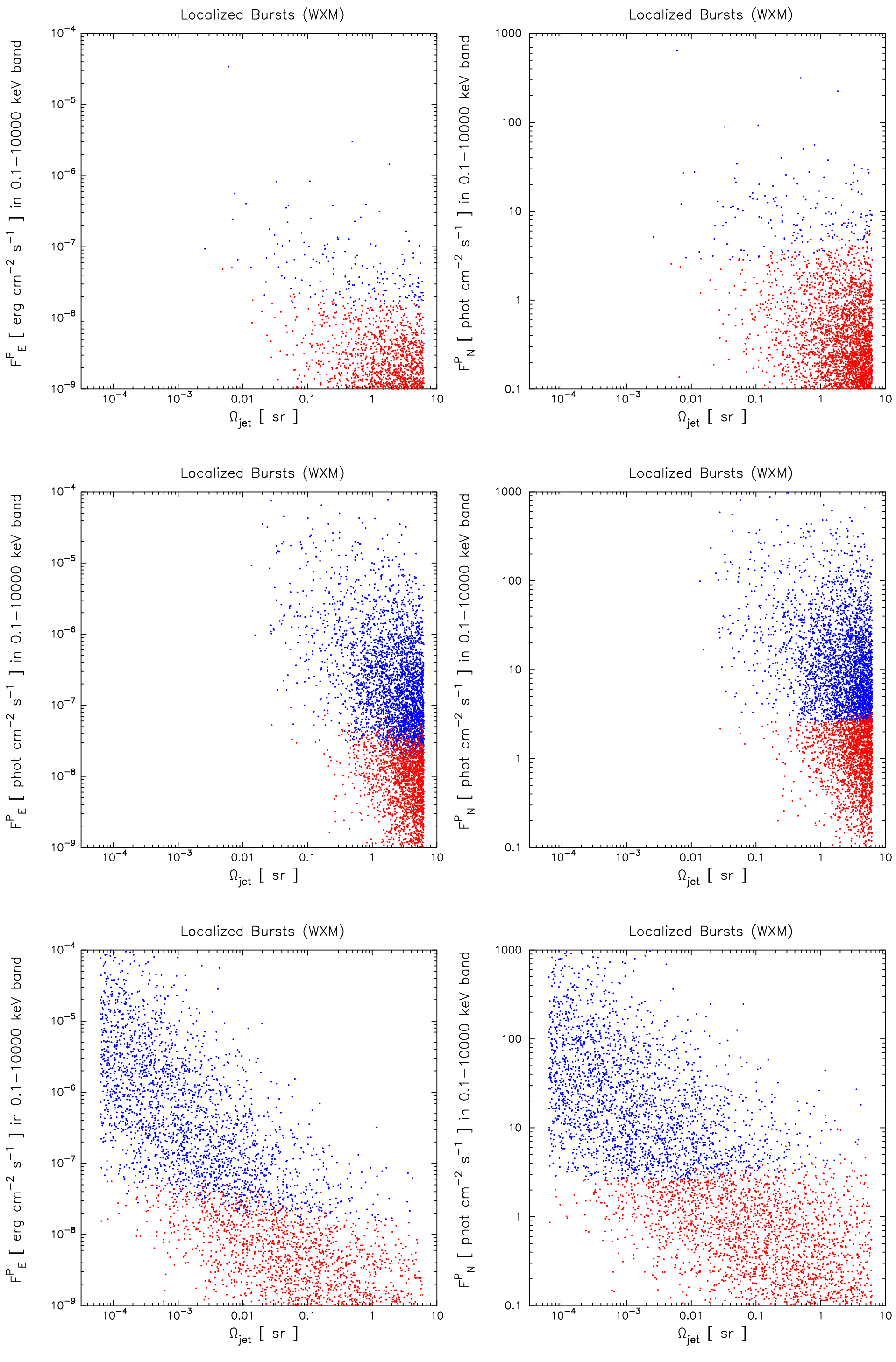

Fig. 10.— Scatter plots of F_N^P versus Ω_{jet}. Upper figure is uniform jet model, left figure is universal jet model pinned to XRF 020903 and right figure is universal jet model pinned to GRB 980326.

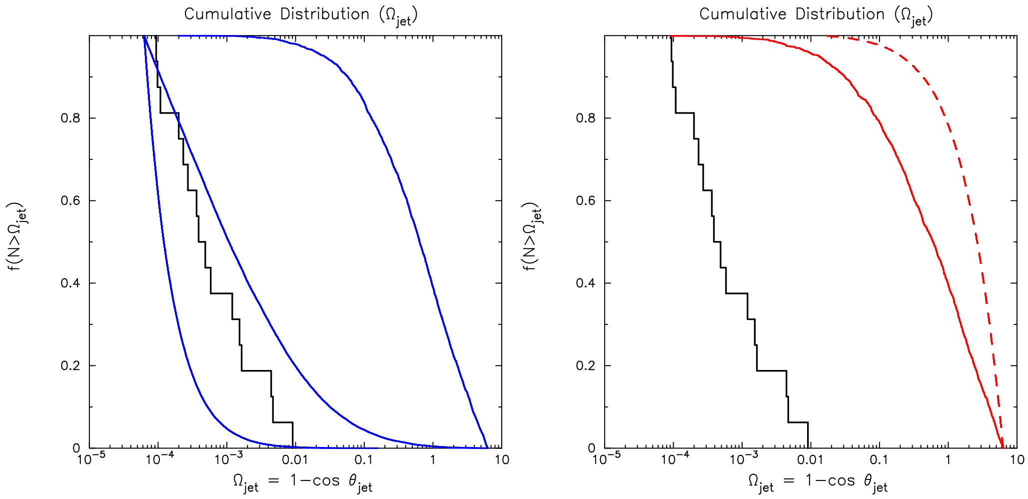

Fig. 11.— Omega cumulative distributions. Upper left panel shows the uniform jet model for $\delta_{sim} = 0$, 1 and 2. Upper right panel shows the two variants of the universal jet model.

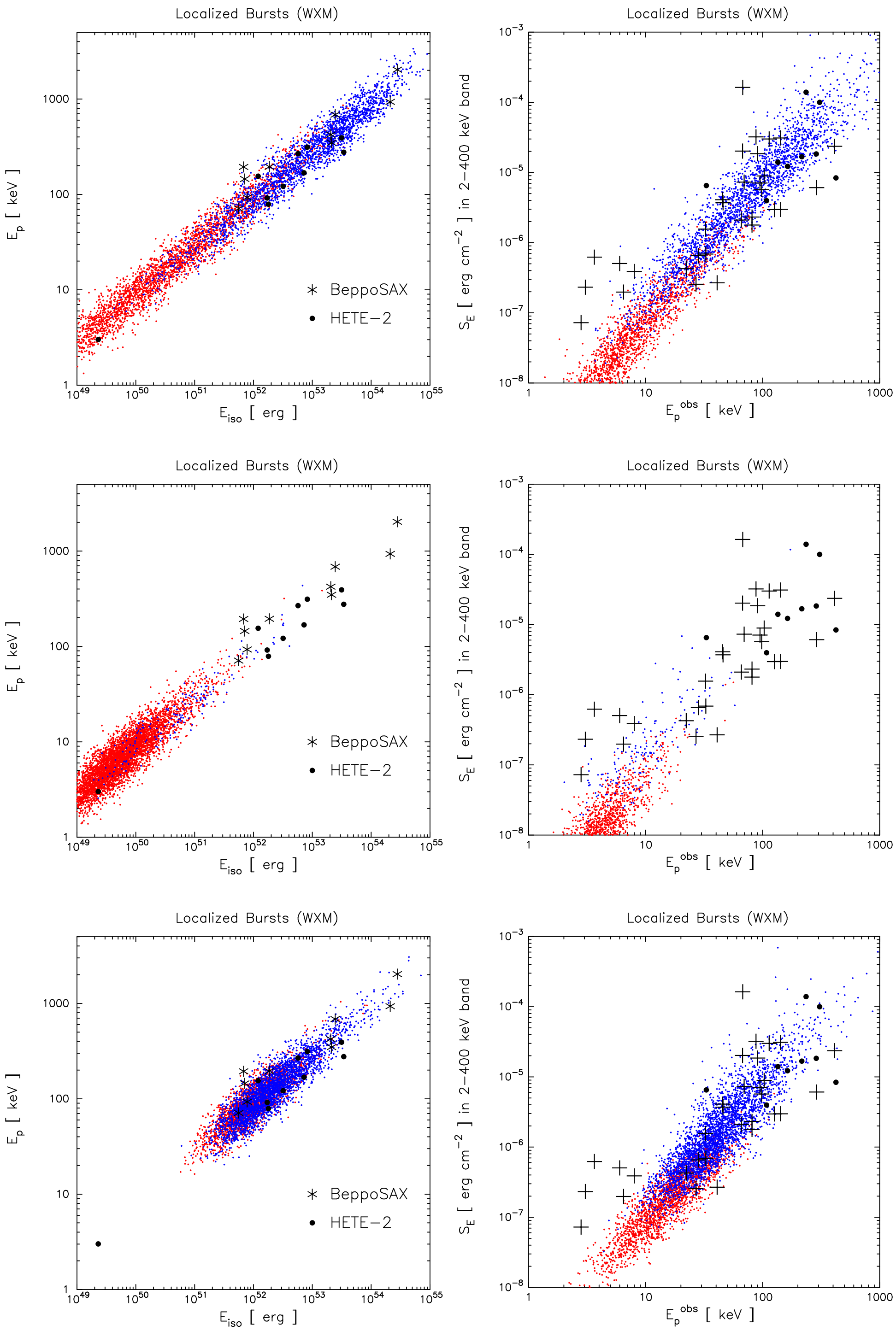

Fig. 12.— Scatter plots of E_{iso} vs. E_p (left column) and E_p^{obs} vs. S_E in 2-400 keV range. Top row is uniform jet model, middle row is universal jet model pinned to XRF 020903 and bottom row is universal jet model pinned to GRB 980326.

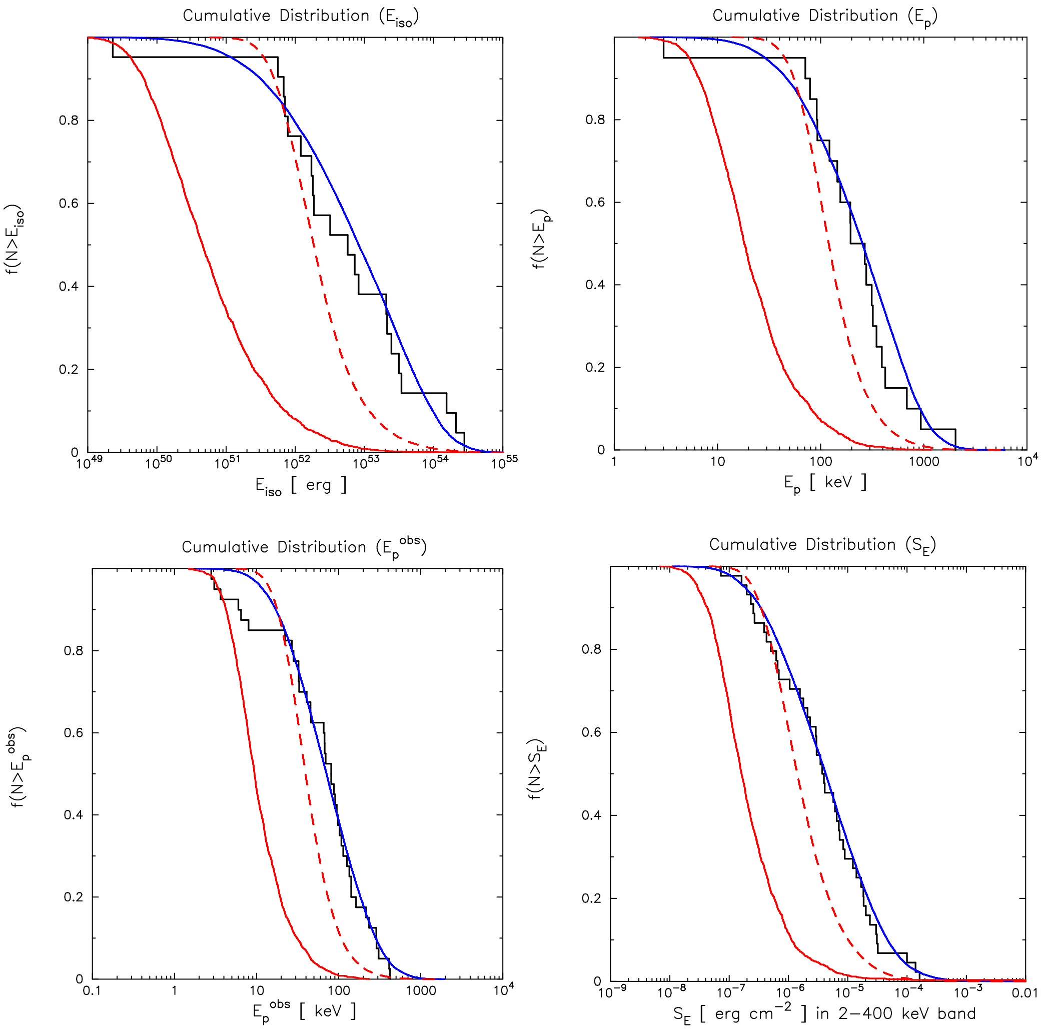

Fig. 13.— Four cumulative distributions. Blue curve is the uniform jet model. Solid red curve is the universal jet model pinned to XRF 020903, while the dashed red curve is the universal jet model pinned to GRB 980326.

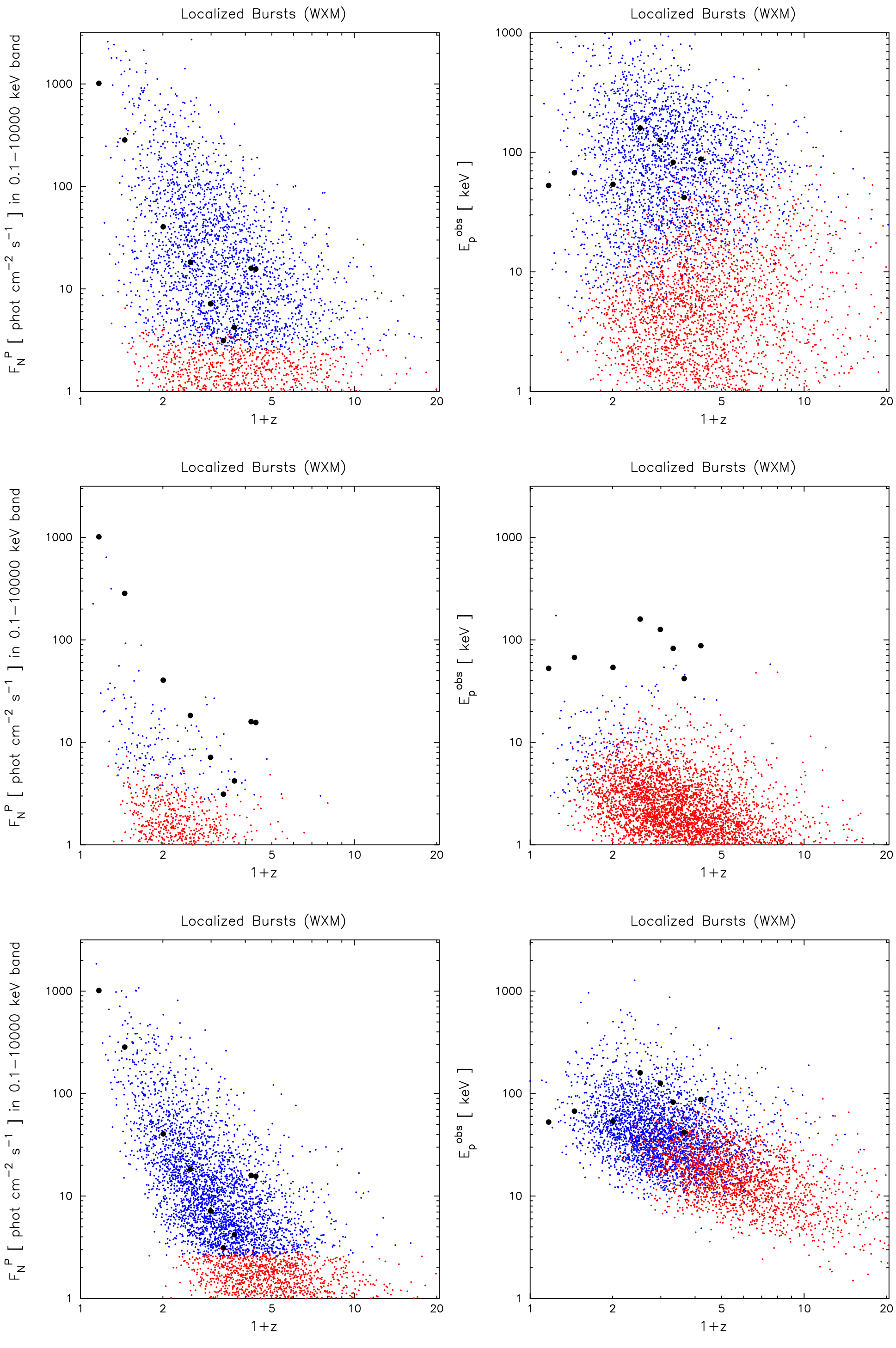

Fig. 14.— Scatter plots of $1 + z$ vs. F_N^P (left column) and E_p^{obs} (right column). Top row is uniform jet model, middle row is universal jet model pinned to XRF 020903 and bottom row is universal jet model pinned to GRB 980326.

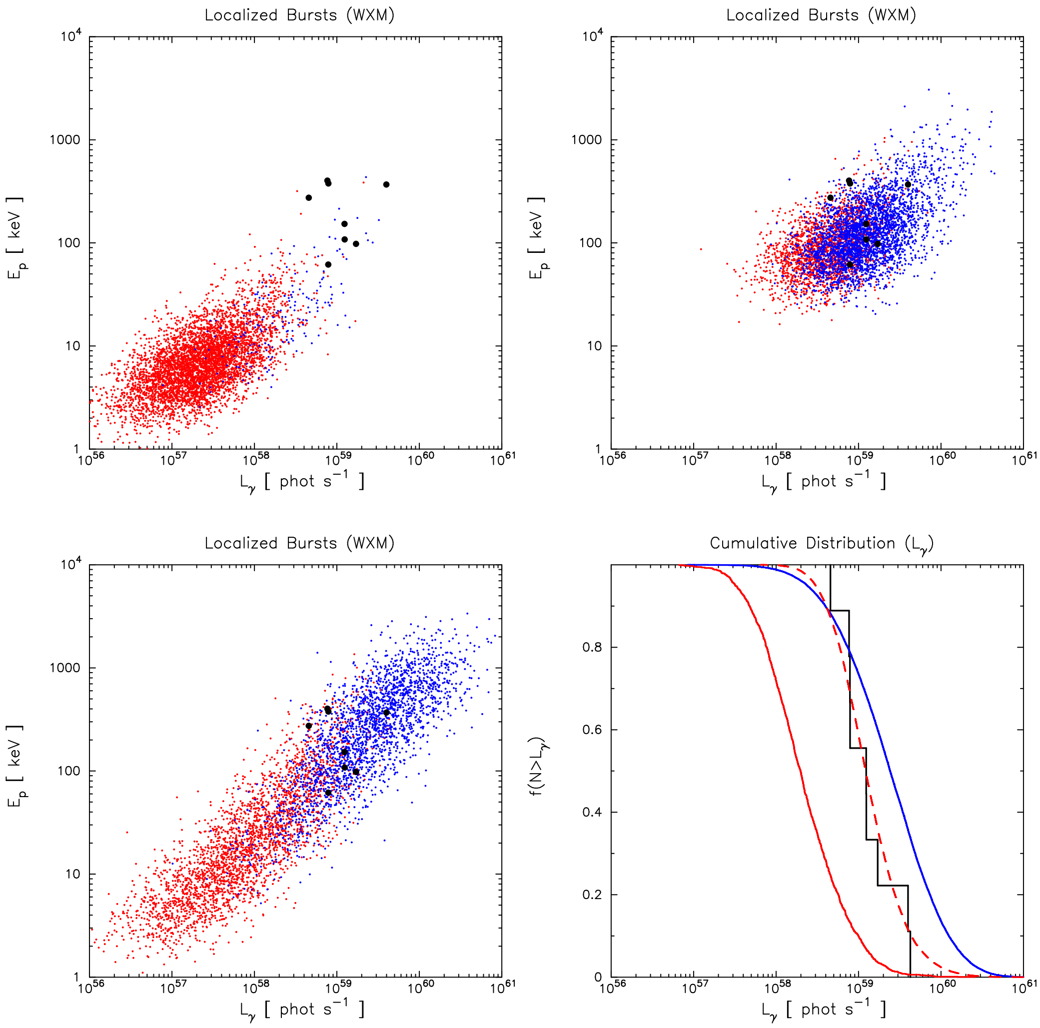

Fig. 15.— Upper figures are scatter plots of L_γ vs. E_p for the universal jet model pinned to XRF 020903 (left) and GRB 980326 (right). Lower left figure is the same for the uniform jet model. Lower right compares the cumulative distributions of the three models against the data.

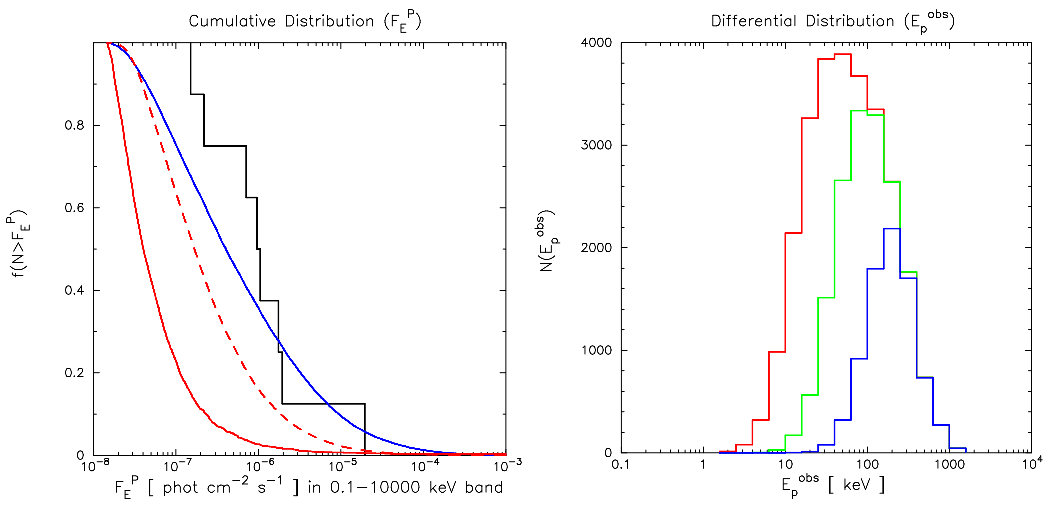

Fig. 16.— Left figures compares the cumulative distributions of F_E^P for the three models. Right figure shows the differential distribution of E_p^{obs} for cuts at $F_E^P = 10^{-6}$, 10^{-7} and 10^{-8} erg cm^{-2} s^{-1}.

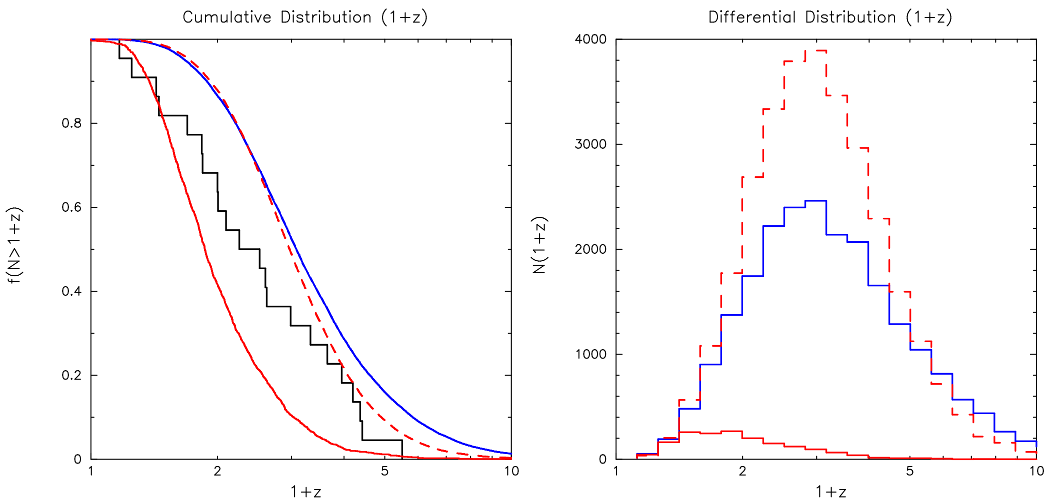

Fig. 17.— Cumulative (left) and differential (right) distributions of GRBs detected by HETE-2 in $1+z$ for the three models.

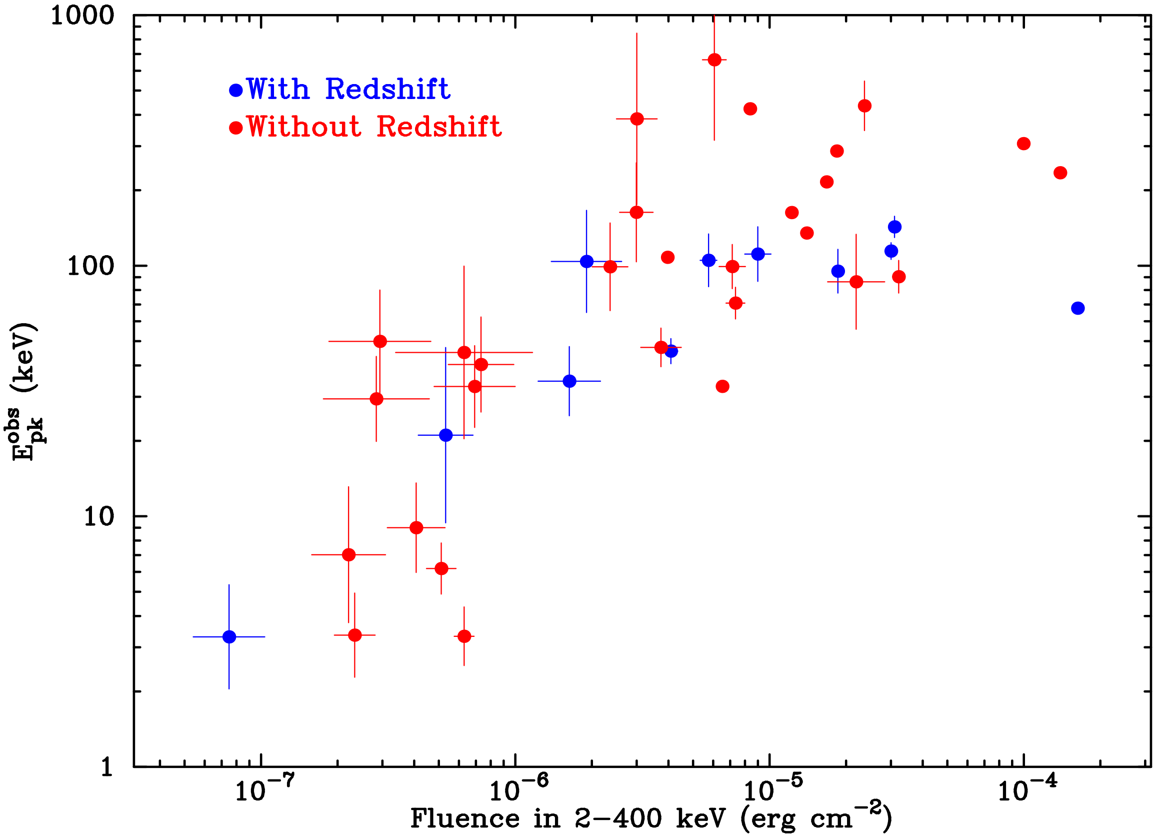

Fig. 18.— Distribution of HETE-2 bursts in the $[S(2-400\mathrm{keV}), E_{\mathrm{peak}}^{\mathrm{obs}}]$-plane, showing the bursts with redshift determinations (blue) and those without (red). The two events with known redshifts in the lower left-hand corner of the figure are XRF 020903 and XRF 030723.

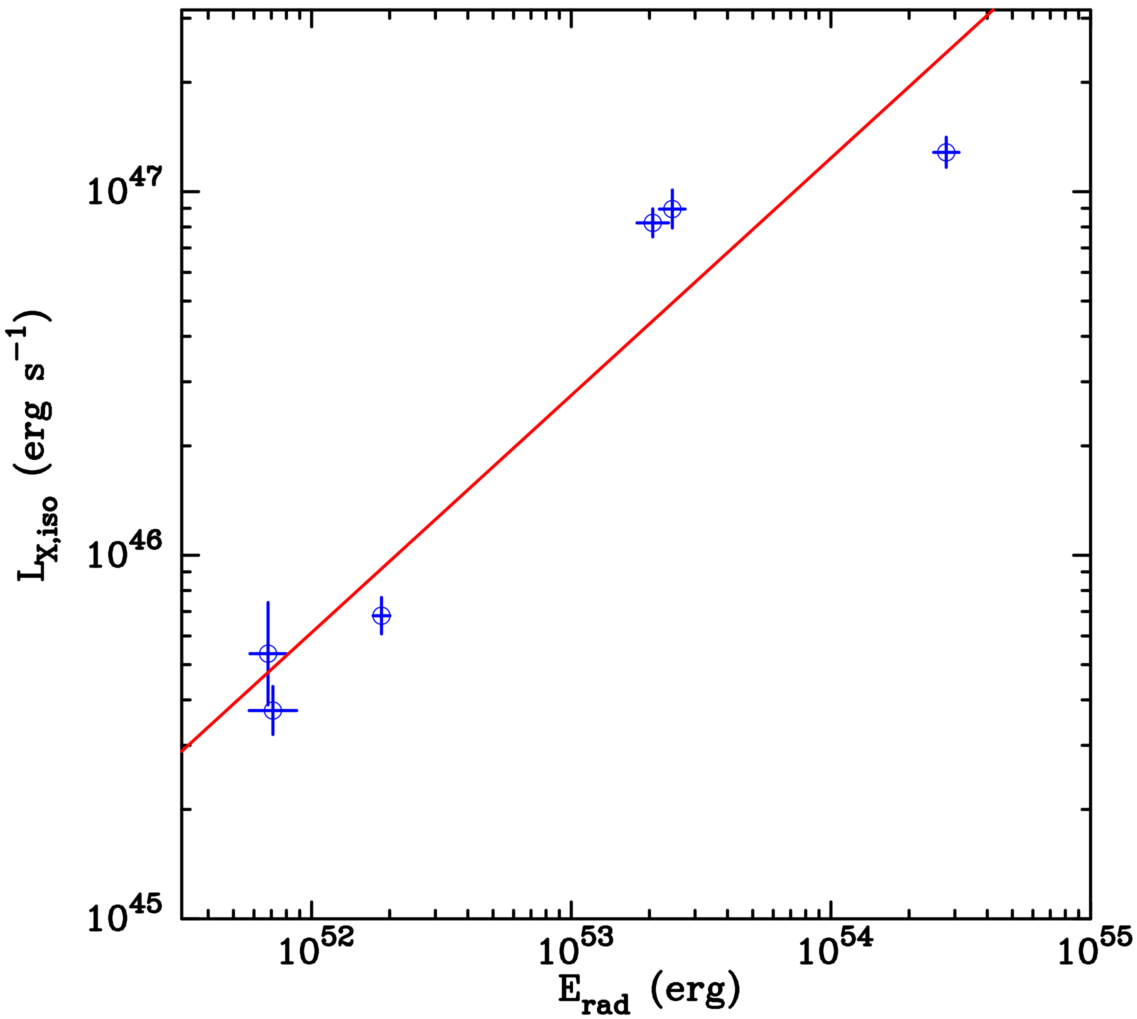

Fig. 19.— Correlation between the isotropic-equivalent γ-ray energy $E_{\rm iso}$ and the X-ray afterglow luminosity $L_{\rm iso}$ at 10 hours after the burst.

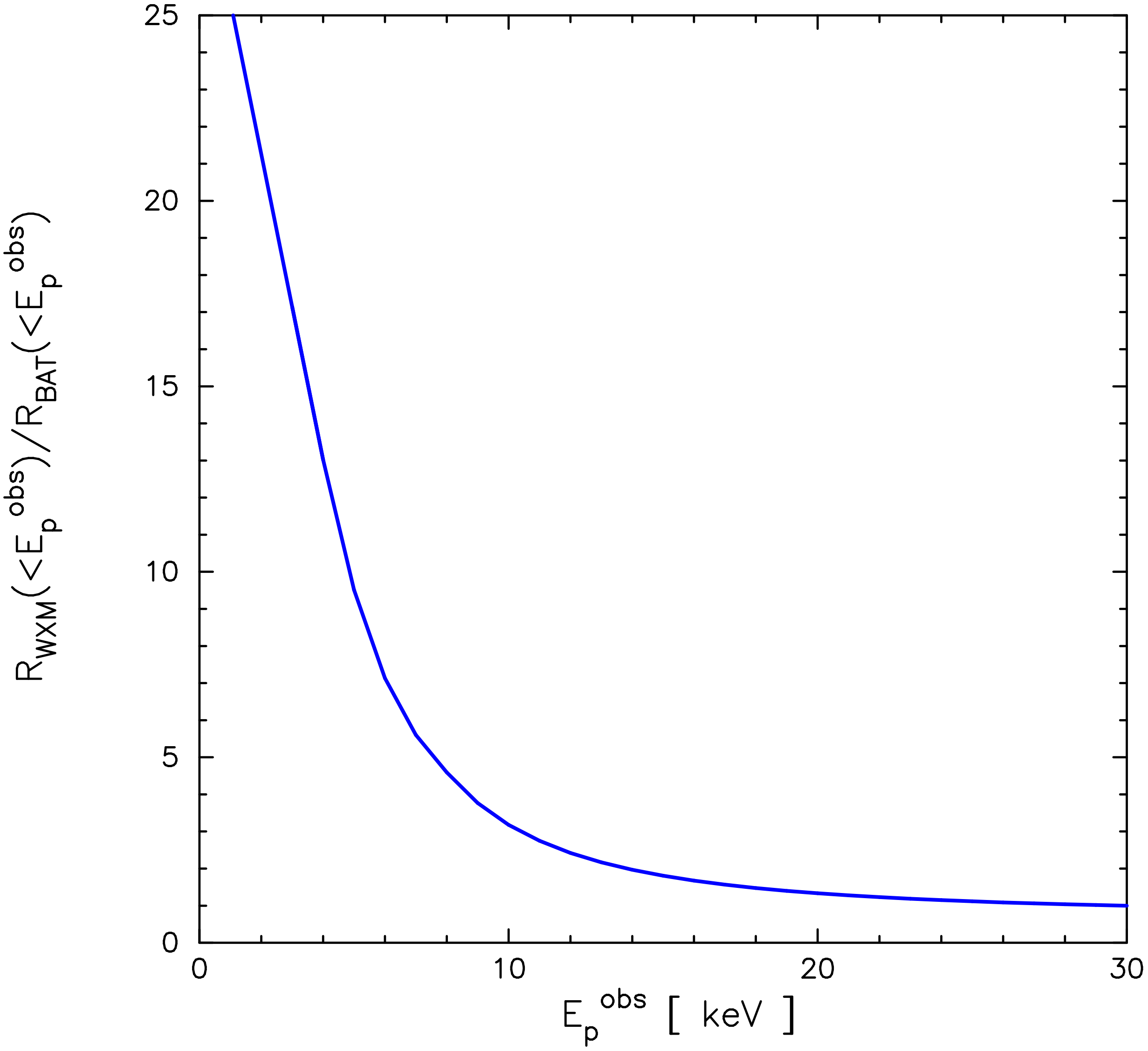

Fig. 20.— Ratio of the rate of detection by WXM on HETE-2 and BAT on *Swift* of XRFs with peak energies less than $E_{\rm peak}$, assuming that the Amati et al. (2002) relation holds for XRFs as well as for GRBs.